SYNTHESIS AND DEVELOPMENT OF NOVEL TETRA-AZA CATALYST PLATFORMS

by

Matthew Charles Fitzsimons

A thesis submitted to the Faculty of the University of Delaware in partial fulfillment of the requirements for the degree of Master of Science in Chemistry and Biochemistry

Summer 2016

SYNTHESIS AND

DEVELOPMENT OF

NOVEL TETRA-AZA

CATALYST PLATFORMS

by

Matthew Charles Fitzsimons

Approved: _____
Joel Rosenthal, Ph.D.
Professor in charge of thesis on behalf of the Advisory Committee

Approved: _____
Murray Johnston, Ph.D.
Chair of the Department of Chemistry and Biochemistry

Approved: _____
George H. Watson, Ph.D.
Dean of the College of Arts & Sciences

Approved: _____
Ann L. Ardis, Ph.D.
Senior Vice Provost for Graduate and Professional Education

ACKNOWLEDGMENTS

I would like to offer my deepest thanks to my friends and family for their unconditional and unending support on this and future endeavors. Especially my parents, Louise and Sean, for all the love they have shown me throughout the years, I could not have done this without them. I also want to thank all of my teachers who have guided my education both inside and outside the classroom. Finally I want to offer a special thanks to Dr. Charlie Russell, who first guided me towards chemistry research, may he rest in peace.

TABLE OF CONTENTS

LIST OF FIGURES

ABSTRACT

Potential tetra-aza catalytic platforms have been synthesized and there electronic structures investigated through various methods. A *tris*(pentafluorophenyl) phlorin derivative was bound to a phosphorous(V) central atom. The complex was characterized with electronic spectroscopy, cyclic voltammetry, differential pulse voltammetry, and ^{1}H NMR spectroscopy. The complex was compared with an analogous phosphorous corrole. A novel *bis*(imino) ligand with a dipyrromethane spacer was developed and bound to several metal centers, including Ni(II) and Zn(II). These complexes and the free-base ligand were characterized with a variety of techniques and structures were confirmed with X-ray crystallography.

Chapter 1

INTRODUCTION

1.1 Global Energy Consumption

Since the mid-1960's the energy consumed globally has more than tripled (figure **1**).[1] This can be attributed to many factors including increasing populations and modernization in different reaches of the world. The global energy portfolio, while diverse, derives most of its energy from naturally occurring carbon-based fuels.[1]

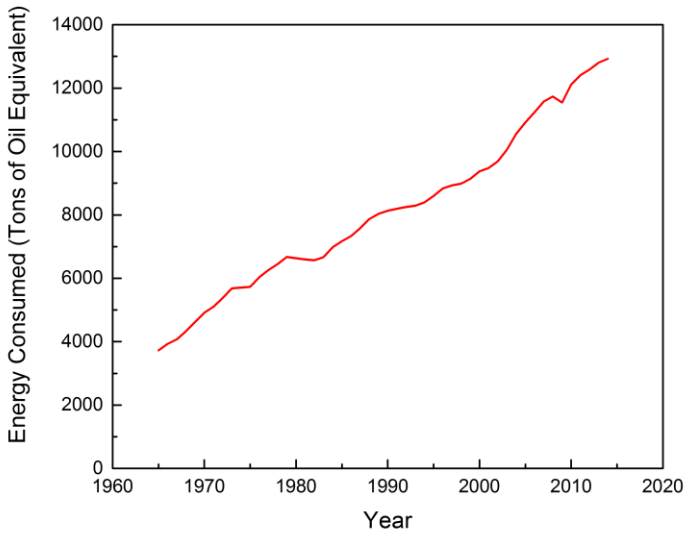

Figure **1**. Global energy consumption from 1965-2014.

In 2014 according to the BP Review of World Energy, over 85 % the world's energy came from carbon-based sources, natural gas, oil, and coal (figure **2**).[1] The prevalence of carbon-based fuels in the global energy portfolio is largely due to their ease to obtain and consume them relative to other sources. Additionally they benefit from the already large infrastructure in place for their consumption.

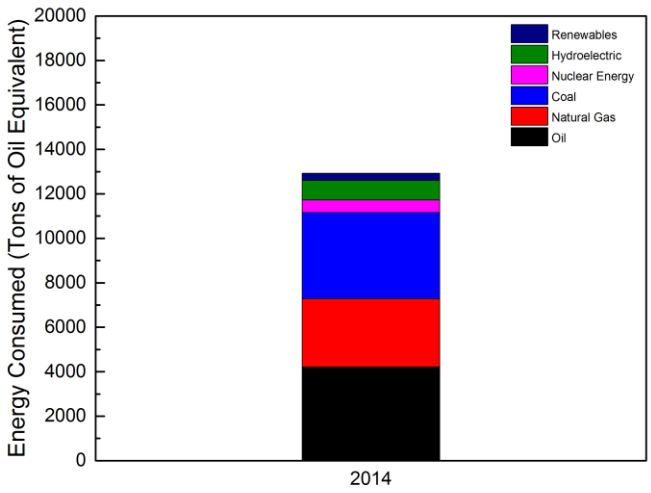

Figure **2**. Global energy consumed by fuel type in 2014.

The combustion of these fuel sources produces carbon dioxide, which is a known greenhouse gas.[2] In conjunction with the increase in global energy consumption, there has been an increase in carbon dioxide emissions over the past half-century (figure **3**).[1] The negative effects of greenhouse gases on the environment have been well noted by groups, like the International Panel on Climate Change.[3]

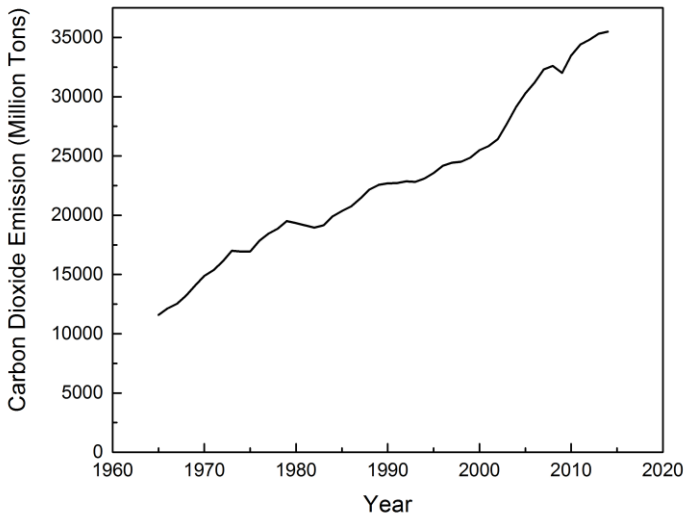

Figure **3**. Global CO_2 emission from 1965-2014.

1.2 Renewable Energy

While there are enough natural fuel reserves to sustain the current rate economic growth for centuries, the concerns over the environmental impact of continued burning of carbon-based fuels has led to an increased interest in developing alternative energy sources. Current levels of atmospheric carbon dioxide are above 400 ppm. The atmospheric concentration of carbon dioxide has increased by over 25 % over the past half-century.[4]

It is widely believed that anthropogenic carbon dioxide is a contributor to climate change. In light of this, there has been a push to increase the global consumption of renewable fuels. Between the years 2013 and 2014, global energy consumption increased by a little under 1 %, the increased consumption of carbon-based fuels all fell beneath this, while nuclear, hydroelectric, and renewables all saw growth greater than the average (figure **4**).[1] Renewables saw the biggest increase

between 2013 and 2014 of 11.98 %. The other non-carbon sources, nuclear and hydroelectric, increased by about 2 %, which is double rate the total consumption increased.

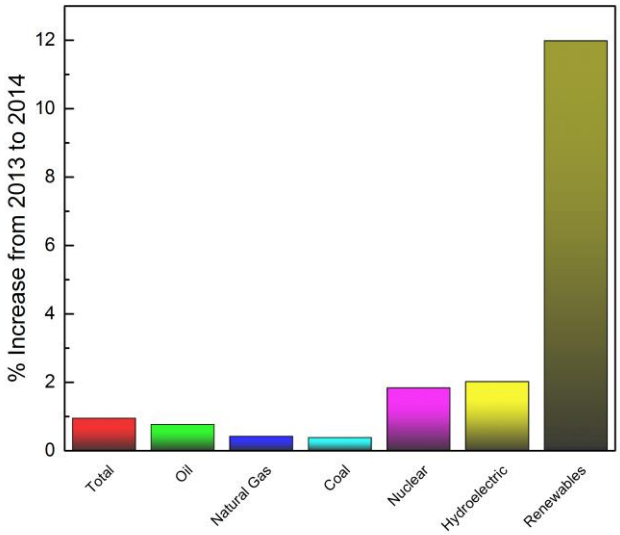

Figure **4**. Percent increase in consumption by fuel type.

1.2.1 Solar Energy

Solar energy is largely consider the most viable renewable energy source. The largest benefit of solar power is scale. The amount of energy produced by the sun that strikes the earth in a day is enough to power the world's energy demands for the entire year. However, there are still significant challenges that need to be overcome before solar energy is a viable alternative to carbon-based fuels. The intermittency of sunlight is one of these challenges. The need for energy is not limited to when the sun shines, like at night. To overcome this, methods of storing energy have been explored

such as battery technologies. One facet of research has taken its inspiration from nature and looks to transfer the energy of the sun into chemical bonds.[5] In nature, during the process of photosynthesis this feat is accomplished through a manganese cluster in photosystem II.[6]

1.2.2 Tetrapyrrole Macrocycles

In addition to storing and transporting energy, the development of cheap and efficient solar cell materials is crucial to the long-term viability of solar energy. Currently the best technologies are expensive multijunction cells with efficiencies above 40 %.[7] Recent work has been in developing low cost dye-sensitized solar cells, with utilize an organic dye to absorb solar radiation. Again taking inspiration from nature, this work has targeted tetrapyrrole macrocycles like that found in chlorophyll, nature's most famous light-harvester. However these cells are not as efficient as their expensive counterparts. Currently the highest achieved efficiencies with these type cells are 12 % achieved by Gratzel.[8]

While for tetrapyrroles, such as porphyrin, their photochemistry is one of their most studied properties. These molecules have been seen in other applications throughout nature. One example is cytochrome *c* oxidase which converts O_2 into water in the process of cellular respiration.[9] This specific example utilizes a metalloporphyrin to activate a small molecule. An application that has been investigated for other energy related applications, like fuel cells. Developing a system that uses the energy absorbed from these molecules to transform small molecules could prove invaluable to the ultimate viability of solar energy in the future.

1.3 Energy-Storing Catalysis

Energy-storing catalysis could prove to be fundamental in the implementation of solar energy. By fueling energetically unfavorable reactions with solar energy, a system is created for storing the solar energy in the chemical bonds created in the reaction. Within this field carbon dioxide reduction has been a specific target. The goal for this is by reducing carbon dioxide to carbon monoxide, it is possible to create a carbon-neutral cycle of fuel consumption. That carbon monoxide can then be used as a carbon feedstock for the Fischer-Tropsch process to generate artificial petroleum.[10] An added benefit to this application of solar fuel is that it does not require a large overhead cost for restructuring existing infrastructure.[11]

Chapter 2

DEVELOPMENT of PHOSPHOROUS PORPHYRNOID COMPLEXES

2.1 Background

Tetrapyrrole macrocycles have been featured prominently throughout nature for light-harvesting processes.[12,13] This has led to the study and derivation of several varieties of tetrapyrrole compounds, such as, porphyrins, corroles, and phlorins. Due to their rich-photophysical properites many of these molecules are of interest for both solar energy harvesting as well as fluorescent bioimaging.[14] Only in recent work has the known library of phlorins been expanded and investigated for such applications.

2.1.1 Phlorin Macrocycle

The phlorin molecule is structurally similar to the more widely studied porphyrin; where a *meso*-positioned sp^2-hybridized carbon is replaced with and sp^3-hybridized carbon.[15-17] The change of this hybridization introduces some multi-electron redox transformations to the macrocycle, which are no observed in analogous phophyrins, but are present in another prophyrinoid, the prophyinogen.[18-20] By altering only one of porphyinoid's *meso*-positions the macrocycle maintains its high degree of conjugation, preserving it photophysics.

2.1.1.1 Phlorin as a Ligand

Often in natural systems, porphyrins can be seen acting as a ligand for various metals.[9] The coordinated atoms can serve two purposes for the new complex: 1) the central atom can facilitate catalytic transformations by accessing a multitude of

oxidation states, 2) the central atom can tune the photophysical properties of the molecule. While the phlorin has been shown to act as a ligand, it has not shown the rich coordination library that porphyrins have. The only previous instance of a coordinated phlorin complex synthesized from a free-base phlorin precursor are a gold(III) and a cobalt(III) phlorin complex.[21-22]

The disparity of coordination chemistries between these two families of porphyrinoids may be their electronic structure. While the porphyrin is diprotic as a free-base and acts as a dianionic ligand, phlorin molecules are triprotic and act as trianions when ligands. Instead, it is useful to compare phlorins to another member of the porphyrinoid family, the corrole.

2.1.2 Corrole Macrocycle

The corrole is another tetrapyrrole macrocycle. Structurally it is similar to the porphyrin, however one of its *meso*-positioned carbons is not present, forming a direct link between two of the pyrrole subunits.[23] Like phlorins, these molecules act a trianions when acting as a ligand. Corrole complexes typically feature a high-oxiadation state central atom.[24] Corroles have absorption features in the red and near-IR regions of the spectrum, which make them suitable for bioimaging applications.[25]

2.1.3 Biological Applications

To maintain usefulness of these compounds for biological applications, the complexes must have a low biotoxicity.[26] Due to this the coordination of corroles to non-toxic elements is desirable. Phosphorous has been of interest to these application

because it has a low biotoxicity and has access to high-oxidation states.[26] Phosphorous tetrapyrroles have also been shown to exhibit fluorescent properties[27] unlike high-oxidation state metal centers, which tend to be nonfluorescent due to low-lying charge transfer states.[28]

Using corrole's coordination chemistry as an inspiration, phlorin chemistry can be opened to a wider host of applications through its own coordination. A coordinated phlorin molecule can offer several advantages to their corrole analogues. As previously mentioned the phlorin sp^3-hybridized *meso*-position carbon atom provides access to multi-electron redox transformations. In addition to this, the modular synthesis of the phlorin free-base provides numerous points of modification, allowing for increased ability to tune the specific characteristics of the target molecule.[15] This is in sharp contrast to corroles which are often synthesized in a one-pot synthesis from pyrrole and aldehyde precursors.[29] This distinction is of particular significance in the field of bioimaging, where modification of a molecule may be necessary to improve biouptake or bioselectivity.

2.2 Synthesis of Tetrapyrrole Macrocycles

2.2.1 Synthesis of *Tris*(pentafluorophenyl)corrole

Tris(pentafluorophenyl)corrole (Cor^F) was synthesized according to a procedure published by Gryko (figure **5**).[29] Pentafluorobenzaldehyde was reacted with pyrrole and trifluoroacetic acid in a neat solution for five minutes. The reaction was dissolved in dichloromethane, and a solution of 2,3-dichloro-5,6-dicyano-1,4-

benzoquinone in tetrahydrofuran and toluene and reacted. The product was purified on a silica column.

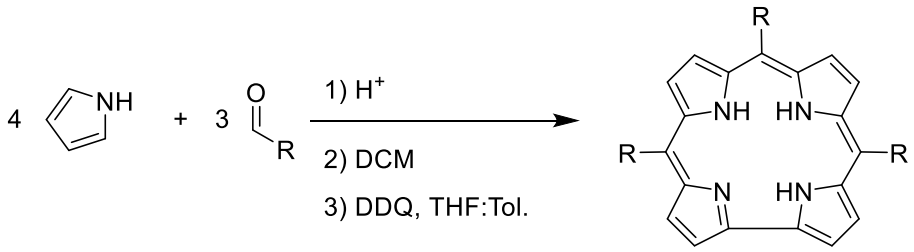

Figure **5**. Scheme of the general (3+4) condensation reaction for corrole synthesis published by Gryko.

2.2.2 Synthesis of *Tris*(pentafluorophenyl)phlorin

Tris(pentafluorophenyl)phlorin was synthesized following a procedure developed by the Rosenthal research lab (figure **6**).[15] A carbonyl and pyrrole were condensed with an acid catalyst to synthesis a dipyrromethane. The dimethyldipyrromethane variant was reacted with ethyl magnesium bromide in dry toluene for one hour under a nitrogen atmosphere. An acid chloride is added to the reaction dropwise and reacts for thirty minutes. The reaction was washed with a solution of ammonium chloride. The organic phase was washed, dried, and purified on a silica column to isolate the product, in this case the acid chloride was pentafluorobenzoyl chloride. The diacyl compound was reduced with sodium borohydride to yield a diol. The diol was washed, dried, and dissolved in dichloromethane to condense with a dipyrromethane with a tertiary central carbon under acidic conditions. The intermediate compound is oxidized with 2,3-dichloro-

5,6-dicyano-1,4-benzoquinone under basic conditions to yield the desired phlorin after purification on a silica column.

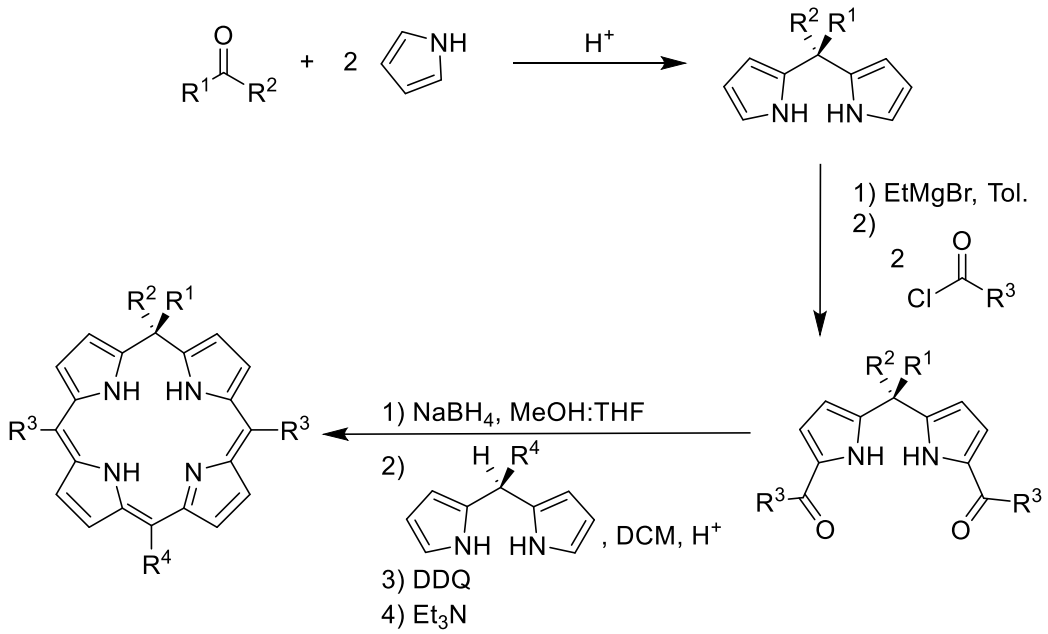

Figure **6**. Scheme of general synthesis for phlorins published by the Rosenthal Lab.

2.3 Synthesis of Phosphorous Macrocycle Complexes

The coordination of phosphorous were synthesized based on the work by Giribabu (figure **7**).[30] The relevant free-base macrocycle was reacted phosphorous(V) oxychloride in dry pyridine at reflux. The product was isolated off of a silica column and confirmed with ^{1}NMR spectroscopy and liquid injection field desorption/ionization mass spectrometry.

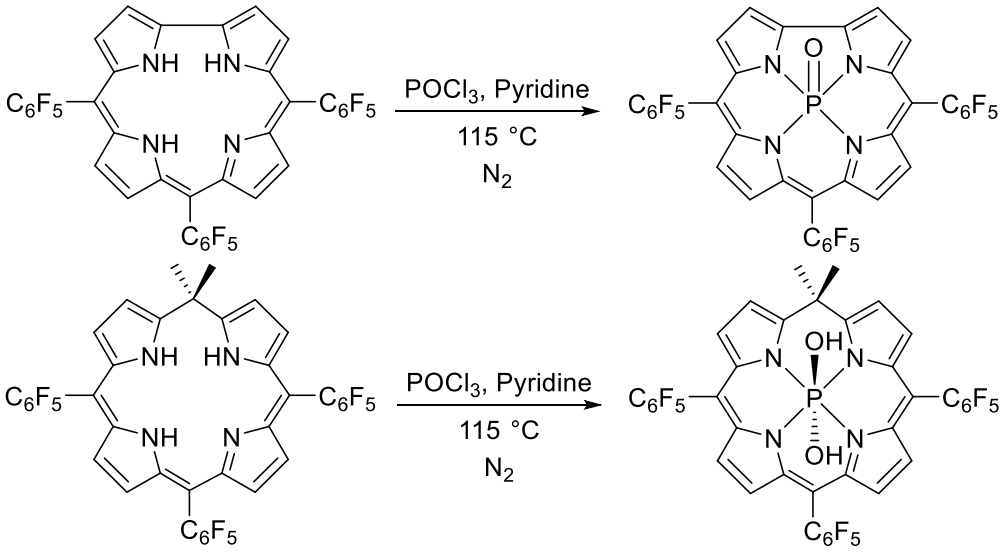

Figure **7**. Synthesis of phosphorous macrocycle complexes.

2.4 Electronic Spectroscopy Studies of Compounds

2.4.1 Background

Electronic spectroscopy is a common characterization technique for the study of porphyrins and porphyrinoids. The extended conjugation of porphyrins and similar porphyrinoids grants them rich features in the visible region of the electromagnetic spectrum. These features are assigned to the attributed to $\pi \rightarrow \pi^*$ transitions within the molecule. The features are categorized as two types, Soret and Q bands. The Soret band is at higher energy, usually around 400 nm. The Q bands are typically found at energies of 500 nm or lower. The Q bands have been shown to represent the transitions from the ground state ($\mathbf{S_0}$) to the first excited state ($\mathbf{S_1}$). Whereas the Soret band is from the transition from the ground state to the second excited state ($\mathbf{S_2}$).[31-33]

2.4.2 Electronic Spectrum of Free-Base Corrole

The electronic spectrum of the free-base *tris*(pentafluorophenyl)corrole was obtained in acetonitrile and dichloromethane (figure **8**). The spectra were comparable with reported spectra for other corroles. The primary feature in the spectra was a sharp Soret band around 400 nm. The spectra both featured several Q-band absorptions between 500 – 700 nm. In the non-polar solvent, dichloromethane, the corrole exhibited a stronger molar absorptivity of 13446 $M^{-1}cm^{-1}$ at 560 nm versus the 9865 $M^{-1}cm^{-1}$ at 564 nm in the polar acetonitrile solvent. These experimental finding are consistent with observations made of the compound in solution. In the solid-state as well as nonpolar solvents the corrole appears purple. However in polar solvents the color shifts to a green hue. This change was not observed phosphorous corrole spectra, taken in dichloromethane and acetonitrile respectively.

A) B)

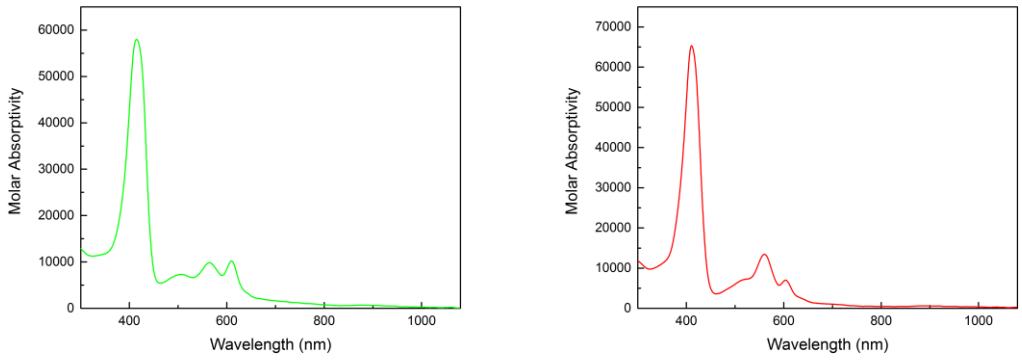

Figure **8**. Electronic spectrum of *tris*(pentafluorophenyl)corrole taken in (**A**) acetonitrile and (**B**) dichloromethane.

2.4.3 Electronic Spectrum of Phosphorous Corrole Complex

The electronic spectrum of the phosphorous corrole complex (figure **9**) showed no noticeable change when solvent polarity was changed. Additionally the free-base corrole spectrum, the soret band of the phosphorous corrole showed no shift. The absorptivity of the Q-bands of the phosphorus complex are enhanced and blue shifted relative to those of the free-base corrole. The most intense absorption of the Q bands is a peak of 22365 $M^{-1}cm^{-1}$ at 580 nm. The blue shift of the Q bands indicates that the HOMO-LUMO gap has increased through the binding of the phosphorous atom. This result is similar to those seen in complexation of Cor^{F} with gallium(III).[34] However, those compounds also showed a red-shifted Soret band by about 20 – 40 nm depending on the metal. This indicates the reduction the $\mathbf{S_0 \rightarrow S_2}$ transition in these compounds, which is not present in this phosphorous complex. Additionally the Q bands remain similar in the spectra from both solvents.

A) B)

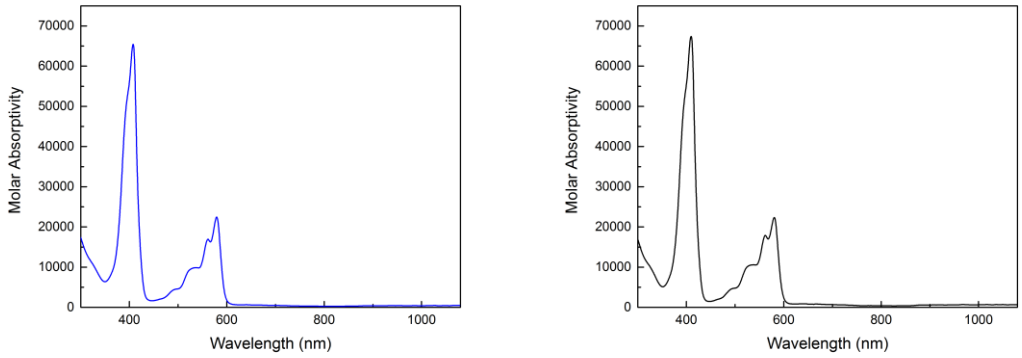

Figure **9**. Electronic spectrum of phosphorous *tris*(pentafluorophenyl)corrole complex taken in (**A**) acetonitrile and (**B**) dichloromethane

2.4.4 Electronic Spectrum of Free-Base Phlorin

The electronic spectrum of free-base phlorin was obtained in acetonitrile (figure **10**). The spectrum shows a Soret band red-shifted relative to the corrole free-base and a Q band also red-shifted relative to the corrole free-base. The lower energy Q bands suggest the HOMO – LUMO gap of the phlorin is smaller than the analogous corrole studied.

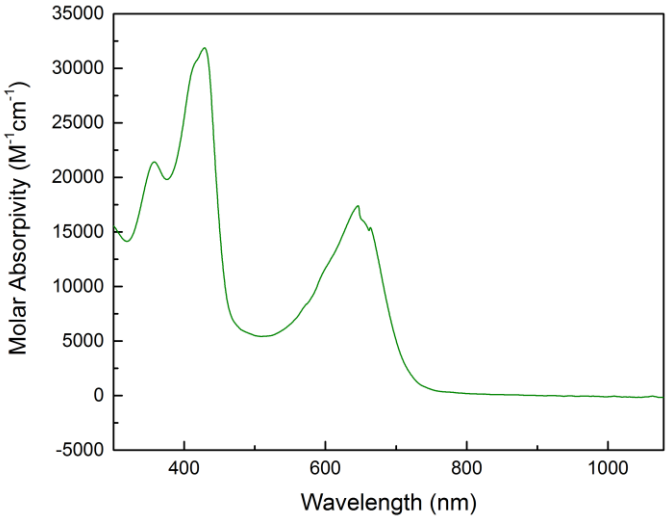

Figure **10**. Electronic Spectrum of Phl^F in acetonitrile.

2.4.5 Electronic Spectrum of Phosphorous Phlorin Complex

The electronic spectrum of phosphorous phlorin complex was obtained in acetonitrile and dichloromethane (figure **11**). The Soret band of the phosphorous complex was red-shifted relative to the free-base compound by 20 nm. A red-shift of over 100 nm was observed in the Q band region of the spectrum as well. These changes indicate the transitions between energy levels are smaller in the phosphorous

complex. In addition the spectrum showed a new low-intensity feature at 547 nm. This feature could be due to a charge transfer between the central phosphorous and phlorin.

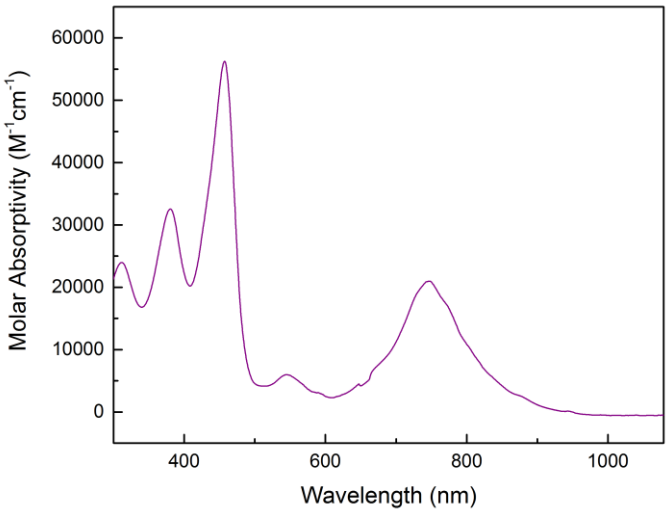

Figure **11**. Electronic spectrum of phosphorous phlorin complex in acetonitrile.

2.5 Electrochemical Studies

2.5.1 Free-Base Corrole

2.5.1.1 Cyclic Voltammetry

The cyclic voltammagram of the free-base corrole was obtained in dichloromethane at rates of 10 mV/s and 100 mV/s. The 100 mV/s scans showed a number of peaks unaccounted for by the corrole, but these peaks were scan rate dependent, as they were not present at the slower 10 mV/s scan rate. The scans at 10

mV/s can be seen below (figure **12**). The scans were referenced to an internal standard of decamethylferrocene (Fc*).

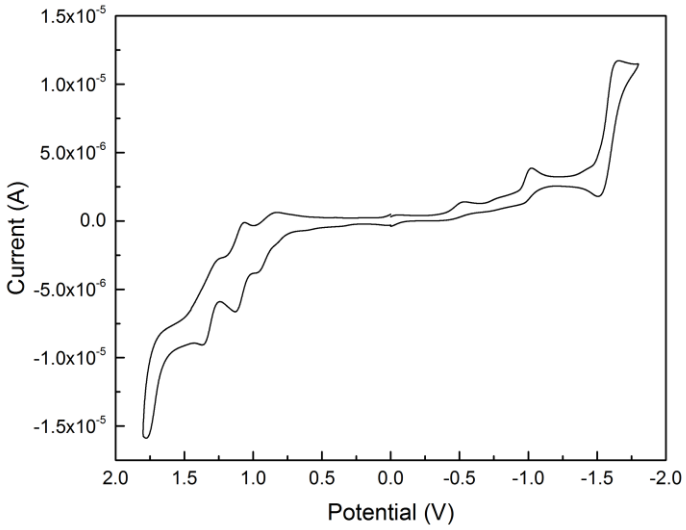

Figure **12**. Cyclic Voltammagram of Cor^F in dichloromethane at 10 mV/s.

2.5.1.2 Differential Pulse Voltammetry

Differential pulse voltammagrams (DPV) of Cor^F were obtained in dichloromethane and referenced with decamethylferrocene as an internal standard (figure **13**). The scans show three large responses, as well as several smaller ones. The smaller response are attributed to adsorption events of electrochemical byproducts of the reductions or oxidations caused by the scans. The larger peaks, one reductive and two oxidative, are attributed to the corrole. The most negative oxidation, at 1.1 V vs Fc^*/Fc^{*+} represents the HOMO of the corrole, whereas the reduction that was

observed at -1.6 V vs Fc^*/Fc^{*+} indicates the LUMO. From these observations the HOMO – LUMO gap for the corrole is 2.6 V.

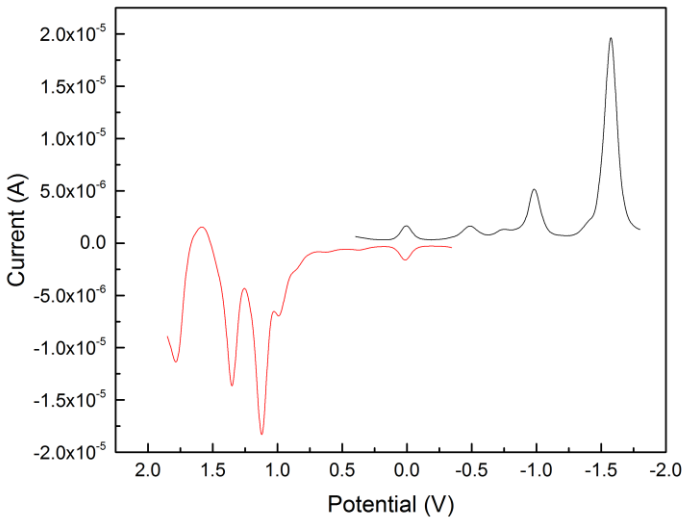

Figure **13**. Differential Pulse Voltammagram of Cor^F.

2.5.2 Phosphorous Corrole Complex

2.5.2.1 Cyclic Voltammetry

The cyclic voltammagram studies of the phosphorous corrole complex were conducted in dichloromethane and acetonitrile at 10 mV/s and 100 mV/s scan rates. The scans at 10 mV/s in dichloromethane are shown below (figure **14**). These scans show one reversible oxidative feature at 1.2 V vs. Fc^*/Fc^{*+}. It also shows two reductive features. The least negative feature comes in at -1.1 V vs. Fc^*/Fc^{*+} and shows reversibility. The other feature is not reversible at -1.6 V vs. Fc^*/Fc^{*+}. Compared to the scans of the free-base corrole, this compound's redox features were

more reversible, indicating a greater stability of in various oxidation states. The scans of the phosphorous complex also show a shift towards more positive potentials. This is due to the electron deficient phosphorous(V) central atom with drawing electron-density from the corrole.

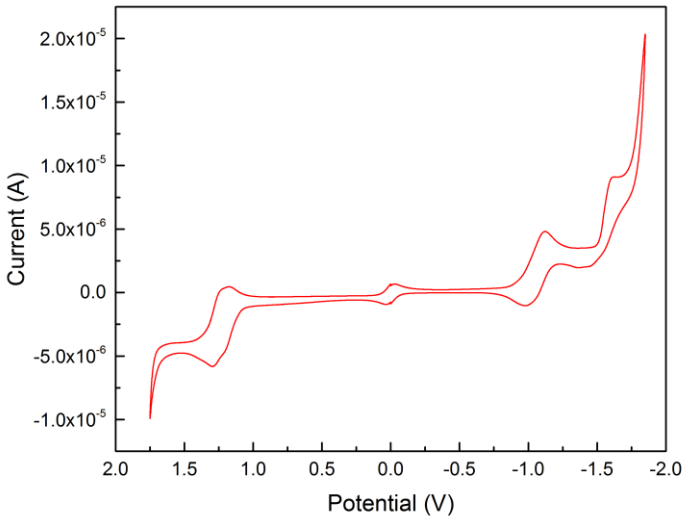

Figure **14**. Cyclic Voltammagram of Phosphorous Corrole Complex.

2.5.2.2 Differential Pulse Voltammetry

The differential pulse voltammagrams of the phosphorous corrole complex were recorded in dichloromethane with decamethylferrocene as an internal standard (figure **15**). Similar to the cyclic voltammetry studies of this compound, the scans do not show responses from byproducts of reduction or oxidation. There are three prominent features in the scans, one oxidation and two reductions. The oxidative peak at 1.2 V vs Fc^*/Fc^{*+} appears to be a coalescence of the two oxidations observed in the

scans of the free-base. The cathodic scan shows a larger peak at -1.2 V vs Fc^*/Fc^{*+}, attributed to the P(V/III) couple, due to its larger integration. The smaller peak at -1.6 V vs Fc^*/Fc^{*+}, is attributed to the reduction of the corrole macrocycle. The HOMO-LUMO gap of orbitals on the corrole macrocycle has increased by about 100 mV. This increase is consistent with the blue shift that was observed between the electronic spectra of these compounds.

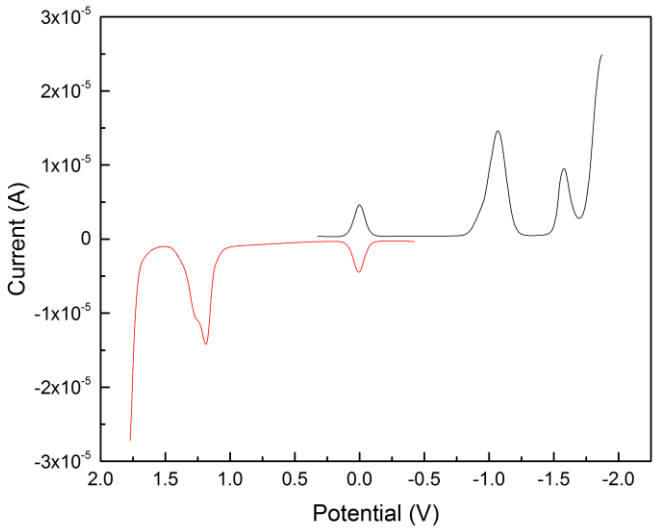

Figure **15**. Differential Pulse Voltammagrams of the Phosphorous Corrole Complex.

2.5.3 Free-Base Phlorin

2.5.3.1 Cyclic Voltammetry

The cyclic voltammagrams of free-base phlorin was taken in acetonitrile and referenced with an internal standard of decamethylferrocene (figure **16**). There are three oxidative features in the anodic scan. The most negative oxidative feature, at

0.75 V vs. Fc^*/Fc^{*+} was reversible as was the reductive feature at 1.2 V vs. Fc^*/Fc^{*+}. The two other reductive features were not reversible.

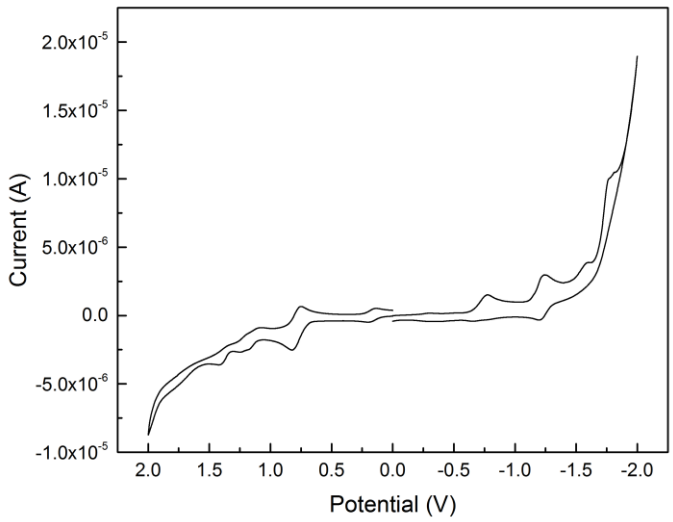

Figure **16**. Cyclic voltammagram of free-base phlorin.

2.5.3.2 Differential Pulse Voltammetry

The differential pulse voltammagrams of free-base phlorin was taken in acetonitrile and referenced with an internal standard of decamethylferrocene (figure **17**). These scans agreed with the cyclic voltammagrams, showing three oxidative features and three reductive features. In the cathodic scan, the peaks are more positive than the reduction peaks of the corrole. From the most negative oxidation and most positive reduction the HOMO-LUMO gap for this molecule was 1.5 V. This smaller gap relative to the free-base corrole, consistent with the redder absorptions of the phlorin.

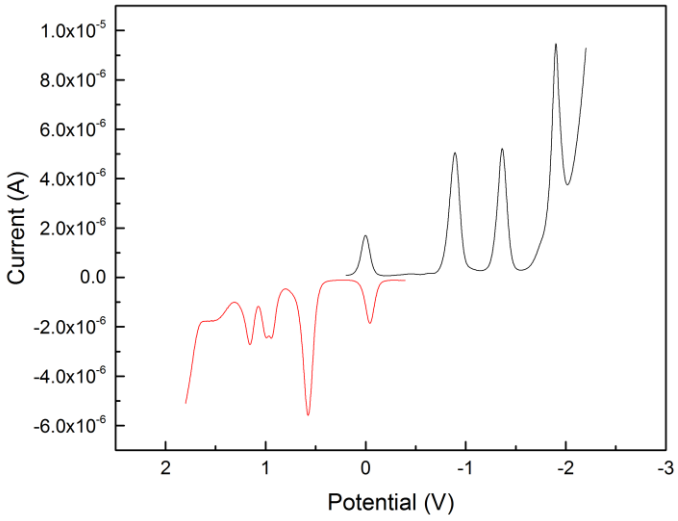

Figure **17**. Differential pulse voltammagrams of free-base phlorin.

2.5.4 Phosphorous Phlorin Complex

2.5.4.1 Cyclic Voltammetry

The cyclic voltammagram scans of the complex were taken in acetonitrile with decamethylferrocene as an internal standard (figure **18**). The scans were taken at a scan rate of 10 mV/s. The addition of the phosphorous can be seen in the addition of the reversible wave at -0.5 V vs. Fc^*/Fc^{*+}. This response from the P(V/III) couple. There were two other cathodic waves, a reversible feature at -1.3 V vs. Fc^*/Fc^{*+} and a nonreversible feature at -1.8 V vs. Fc^*/Fc^{*+}. In the oxidative scan, there were two reversible features. The more negative peak was at 0.9 V vs. Fc^*/Fc^{*+} and the other peak was at 1.2 V vs. Fc^*/Fc^{*+}. Compared to those of the free-base phlorin, the peaks of phosphorous phlorin are more reversible, indicating the phosphorous may be helping to stabilize the various oxidation states of the complex.

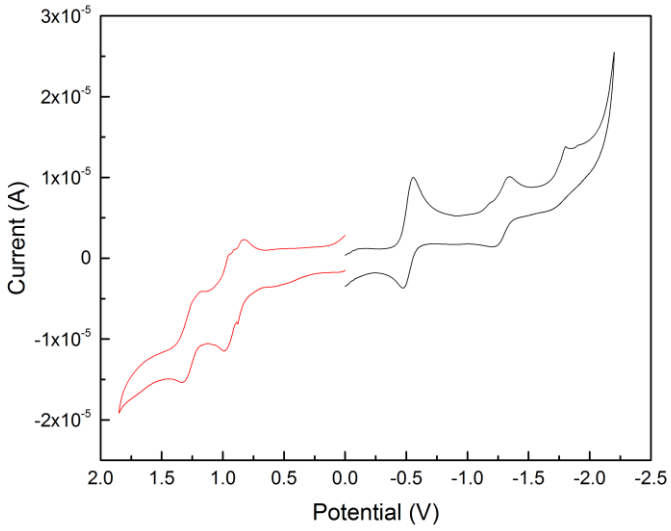

Figure **18**. Cyclic voltammagrams of phosphorous phlorin complex.

2.5.4.2 Differential Pulse Voltammetry

The differential pulse voltammetry scans were acquired in an acetonitrile solution with decamethylferrocene as an internal standard (figure **19**). The anodic scan showed two peaks, at 0.9 V and 1.2 V vs. Fc^*/Fc^{*+}, respectively. In the cathodic scan, there are three peaks at -0.5 V, -1.4 V, and -1.7 V vs. Fc^*/Fc^{*+}. The peak at -0.5 V is likely the P(V/III) couple due to its larger size, relative to other peaks. On the anodic scan, it appears that the two most positive peaks from the free base have coalesced to yield the peak at 1.2 V vs. Fc^*/Fc^{*+}. The oxidative feature from the free-base DPV at 0.6 V appears to have been shifted in the positive direction through the binding of phosphorous by 300 mV. This is consistent with electron-poor phosphorous(V) center pulling electron-density away from the macrocycle. This is also reflected in the cathodic scan, where peaks also appear shifted in the positive direction although by about 100 mV. From these scans we can approximate that the

HOMO-LUMO gap of the molecule is approximately 1.4 V, which is consistent with the red shift observed between the Q-bands of the free-base and phosphorous complex.

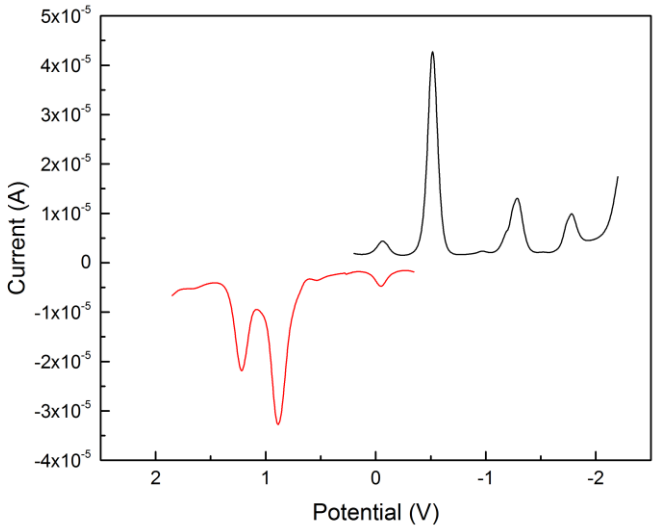

Figure **19**. Differential pulse voltammagrams of phosphorous phlorin complex.

2.6 Emmission Studies

The emissions of the phosphorous complexes were compared to access the phlorin complexes viability for fluorescent bioimaging applications. Analogues of the phosphorous corrole have already been shown to fluoresce and were studied for such applications.

2.6.1 Emmission of Phosphorous Phlorin Complex

The emission of the phosphorous phlorin complex was studied in acetonitrile. The quantum yield of this complex was determined by comparison with a *tris*(bypyridine)ruthenium(II) chloride standard. The compound was exited at 420 nm,

at the foot of the Soret band, and at 700 nm, the foot of the Q-band. The quantum yield of the phosphorous complex fluorescence was determined to be 0.0027 when excited at 420 nm, and no fluorescence was observed from the compound when excited at 700 nm. Similar results have been reported with the free-base phorin, where it is believed the sp^3-hybridized *meso* position provides additional degrees-of-freedom that enable non-radiative decay pathways. Through the ^{1}H NMR studies of the phosphorous complex however, we observe two distinct peaks for the methyls connected to this sp^3-hybridized center, meaning at room temperature these protons are not interchangeable on an NMR timescale. Whereas these same protons in the free-base NMR spectrum appear as one resonance. This suggests that the degrees-of-freedom present in the free-base are restricted when phlorin binds phosphorous. The phosphorous complex was investigated for other non-radiative decay pathways, specifically singlet oxygen activation.

2.7 Singlet Oxygen Study

The phosphorous phlorin complex was tested for singlet oxygen activation following a procedure developed by Martin.[35] A solution of the compound was prepared in methanol with 1,3-diphenylisobenzofuran. 1,3-diphenylisobenzofuran is a fluorescent molecule that reacts with singlet oxygen to yield an nonfluorescent molecule. Tracking the decay of fluorescence from the furan allows the singlet oxygen generation of the complex to be monitored. The quantum yield of singlet oxygen generation was determined by referencing a known singlet oxygen sensitizer, *tris*(bipyridine)ruthenium(II) chloride. To accommodate for different solution absorbencies, calibration curves were developed to normalize results across solutions. The solution was prepared with the sensitizer and furan in methanol. The solution was

then exposed to 450 nm light at various time intervals. The decays of each solution can be seen in figure **20**. The phosphorous complex did not show any appreciable ability to sensitize singlet oxygen relative to a blank which did not contain any sensitizer.

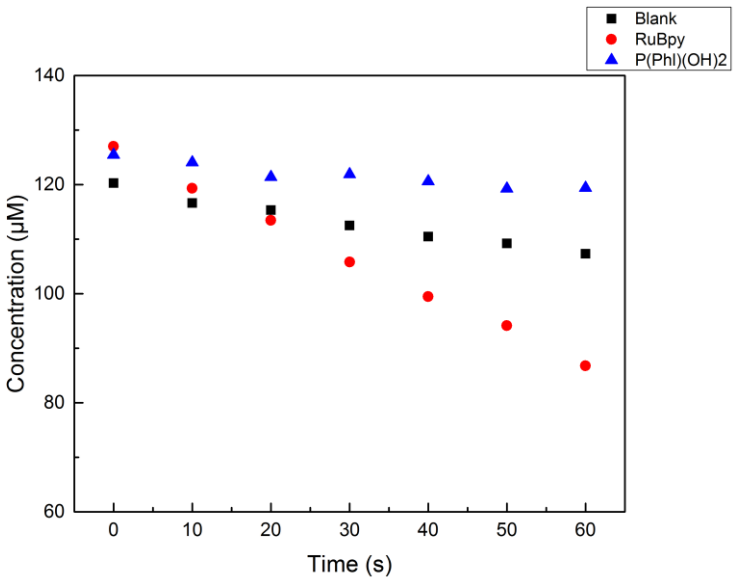

Figure **20**. Decay of furan concentration with various $^1O_2$ sensitizers.

2.8 Summary

This study served to expand the scope and understanding of the phlorin molecules capacity to act as a ligand. Because of their similar electronic structure, the corrole macrocycle was used as an inspiration for exploring this chemistry. Like the corrole, phlorin was used successfully as a ligand on an electron deficient central atom, phosphorous(V). The compounds were studied using spectroscopic and electrochemical techniques to assess the electronic structure of each for comparison.

Through these studies, the effects of the phosphorous central atom on the macrocycles was determined to be similar. Through NMR spectroscopy and mass spectrometry it was determined that the secondary ligands of the phosphorous atoms were different between the compounds. This could indicate a nuanced difference between the electronic structures of the compounds.

Previous reports have shown phosphorous corrole compound have utility as a fluorescent bioimaging probe. Consequently the phosphorous phlorin molecule was investigated for similar properties. However, emission experiments showed the molecule relaxed through a non-radiative process. Dues to the molecules apparent rigidity, decay methods such as vibrational relaxation seemed unlikely. Therefore the molecule was investigated as a singlet oxygen sensitizer. However, the phosphorous complex did not generate an appreciable amount of singlet oxygen in this study.

One of the differences between the two phosphorous complexes is their secondary ligands. It is possible that the hydroxyl ligands of the phosphorous phlorin complex provide the degrees-of-freedom needed for the complex to relax from the excited state without undergoing an emissive process. This is in contrast to the phosphorous corrole complex which is supported by an oxo ligand, which provides less degrees-of-freedom.

2.9 Experimental

2.9.1 General Synthetic Methods

Reactions were carried out under open air unless otherwise specified. Reactants and solvents were obtained from Sigma-Aldrich, Fisher, Strem, Acros, or

Cambridge Isotopes Laboratories. Chemicals were used as obtained unless otherwise specified.

2.9.2 Spectroscopic Methods

NMR spectra were obtained at room temperature. Proton and carbon spectra were obtained referenced to residual deuterated solvent peaks (^{1}H: CD_3CN, $\delta = 1.94$; $CDCl_3$, $\delta = 7.26$; ^{13}C: CD_3CN, $\delta = 1.32, 118.26$; $CDCl_3$, $\delta = 77.16$). All chemical shifts are reported with standard δ notation in parts-per-million. UV/visible spectra were obtained at room temperature on a StellarNet CCD array UV-vis spectrometer using quartz cuvettes with pathlength of 1 cm. Spectra were obtained at room temperature. Electrochemical studies were preformed using a CHI-620D potentiostat/galvanostat. Cyclic voltammetry (CV) and differential pulse voltammetry (DPV) were performed in a nitrogen glovebox with a three electrode set-up. CV and DPV scans were recorded with a glassy carbon working electrode, a platinum wire counterelectrode, and a silver wire quasi-reference electrode. Experiments were performed with 0.1 M solution of tetrabutylammonium hexafluorophosphate in either acetonitrile or dichloromethane. Potentials were referenced to standard hydrogen electrode using an internal standard of decamethylferrocene.

2.9.3 Synthesis of 5,5-Dimethyldipyrromethane

Distilled pyrrole (176 mL, 2.54 mol) was added to the reaction flask. The reaction flask was sealed with a septa and sparged with N_2. Acetone (7.4 mL, 0.100 mol) was added to the flask using a syringe. Trifluoroacetic acid (0.75 mL, 0.010

mol) was added to the reaction via syringe. The mixture reacted for five minutes. A sodium hydroxide solution was added to the reaction. Ethyl acetate extracted the mixture. The organic layer was rinsed with brine and water twice. The organic phase was dried over sodium sulfate and concentrated *in vacuo*. The mixture was purified with a vacuum distillation. The product was collected as a white wax-like solid. Yield: 11.480g (65 %). ^{1}H NMR (400 MHz, $CDCl_3$) δ 7.69 (*s*, 2H, H-N), 6.603 (*dd*, J_A = 4.0 Hz, J_B = 2.8 Hz, 2H, 5-pyrrole H), 6.141 (*dd*, J_A = 3.2 Hz, J_B = 2.8 Hz, 2H, 3-pyrrole H), 6.101 (*m*, 2H, 4-pyrrole H), 1.638 (*s*, 6H, *meso*-methyl).

2.9.4 Synthesis of 2,2'-*Bis*(pentafluorophenylacyl)-5,5-dimethyldipyrromethane

Dipyrromethane (1.742 g, 9.90 mmol) added to a Schleck flask and dissolved in dry toluene (100 mL). Ethyl magnesium bromide solution in tetrahydrofuran (54 mL, 0.513 mol) was added to the reaction dropwise via an addition funnel. The reaction stirred for one hour. A solution of pentafluorobenzoyl chloride (3.6 mL, 0.0251 mol) in dry toluene (10 mL) was added via addition funnel. The mixture reacted for thirty minutes. A saturated solution of ammonium chloride (150 mL) was added to the reaction. The organic phase was separated and washed with water (2x) and brine (2x). Organic phase was dried over sodium sulfate and concentrated *in vacuo*. The reaction mixture was purified on a silica column using a 10:1 mixture of hexane and ethyl acetate eluent. The collected fraction was recrystallized from dichloromethane into hexanes. Yield: 0.978 g (31%). ^{1}H NMR (400 MHz, $CDCl_3$) δ

9.632 (*s*, 2H, H-N), 6.658 (*m*, 2H, 4-pyrrole H), 6.242 (*dd*, J_A = 3.9 Hz, J_B = 2.8 Hz, 2H, 3-pyrrole H), 1.800 (*s*, 6H, *meso*-methyl).

2.9.5 Synthesis of 10,15,20-*Tris*(pentafluorophenyl)-5,5-dimethylphlorin (Phl^F)

Bis(pentafluorophenylacetyl)-5,5-dimethyldipyrromethane (283 mg, 0.50 mmol) dissolved in a mixture of tetrahydrofuran (30 mL) and methanol (10 mL). Sodium borohydride (956 mg, 25.3 mmol) was added to the reaction flask and stirred for two hours. The reaction was quenched with water (40 mL). The reduced reactant was extracted from the aqueous phase with dichloromethane. The organic solution was washed with brine (2x) and water (2x). The organic phase was dried over sodium sulfate. The solution was concentrated *in vacuo*. The residue was dissolved in dichloromethane (200 mL). *Bis*(pentafluorophenylacyl)dipyrromethane (160 mg, 0.51 mmol) was added to the reaction. Trifluoroacetic acid (1.6 mL) was added to the reaction, and reaction stirred for fifteen minutes. 2,3-Dichloro-5,6-dicyano-1,4-benzoquinone (168 mg, 0.764 mmol) was added to the reaction followed by triethyl amine (14 mL). The reaction stirred for thirty minutes. The reaction mixture ran through a silica plug and concentrated *in vacuo*. The product was purified on a silica column with a 5:1 mixture of hexanes and ethyl acetate. Yield: 694 mg (48 %). ^{1}H NMR (400 MHz, $CDCl_3$) δ 7.355 (*d*, *J* = 5.2 Hz, 2H, pyrrole H), 7.119 (*d*, *J* = 4.8 Hz, 2H, pyrrole H), 6.957 (*d*, *J* = 4.0 Hz, 2H, pyrrole H), 6.811 (*d*, *J* = 3.6 Hz, 2H, pyrrole H) 1.530 (*s*, 6H, methyl).

2.9.6 Synthesis of $P(Phl^F)(OH)_2$

Phlorin (128 mg, 0.153 mmol) dissolved in distilled pyridine (5 mL) in a Schleck flask. The flask was sparged with N_2 for five minutes. Phosphorous(V)

oxychloride (1.8 mL, 7.4 mmol) was added to the flask dropwise via syringe. The mixture was heated to 115 °C and reacted for five hours. The mixture turned brown-red in color. The solvent was removed under vacuum. The brown residue was dissolved in dichloromethane and washed twice with water and brine. The organic layer was dried over sodium sulfate. The mixture was added to a silica column and eluted with a 7:3 mixture of hexanes and ethyl acetate. The polarity was increased to pure ethyl acetate. The product was collected as a dark red band. Yield: 90. mg (65 %). ^{1}H NMR (400 MHz, CD_3CN) δ 8.174 (*d, J* = 4.4 Hz, 2H, pyrrole H), 7.563 (*d, J* = 4.4 Hz, 2H, pyrrole H), 7.435 (*d, J* = 4.4 Hz, 2H, pyrrole H), 7.151 (*d, J* = 4.0 Hz, 2H, pyrrole H), 2.623 (*s,* 3H, *meso*-methyl), 0.253 (*s*, 3H, *meso*-methyl).

2.9.7 Synthesis of *Tris*(pentafluorophenyl)corrole (Cor^F)

Pentafluorobenzaldehyde (0.76 g, 4.0 mmol) was added to a flask and heated to 40 °C to melt the compound. A solution of trifluoroacetic acid (0.1 mL) in dichloromethane (0.9 mL) was added to the reaction flask. Pyrrole (0.42 mL, 6.0 mmol) was added to the reaction mixture dropwise and the solution turned dark immediately. The mixture reacted for fifteen minutes at room temperature. Dichloromethane (10 mL) was used to dilute the reaction. A solution of 2,3-dichloro-5,6-dicyano-1,4-benzoquinone (1.1 g, 4.8 mmol) in a 1:1 mixture of tetrahydrofuran and toluene (8 mL). The reaction stirred for five minutes at room temperature. The product was purified on a silica column with a 2:3 eluent mixture of dichloromethane and hexanes. Yield: 103 mg (13 %). ^{1}H NMR (400 MHz, $CDCl_3$) 9.096 (*d, J* = 4.0 Hz,

2H, pyrrole H), 8.788 (*d*, *J* = 4.8 Hz, 2H, pyrrole H), 8.609 (*d*, *J* = 4.4 Hz, 2H, pyrrole H), 8.555 (*d*, *J* = 2.8 Hz, 2H, pyrrole H).

2.9.8 Synthesis of P(Cor^{F})

Tris(pentafluorophenyl)corrole (100 mg, 0.126 mmol) dissolved in distilled dry pyridine (5 mL) in a Schleck flask. The flask was sparged with N_2 for five minutes. Phosphorous(V) oxychloride (1.8 mL, 19.3 mmol) was added to the flask dropwise via syringe. The mixture was heated to 115 °C and reacted for one hour and thirty minutes. The mixture turned pink in color. The solvent was removed under vacuum. The residue was purified on a silica column with a 7:3 mixture of hexanes and ethyl acetate eluent. The polarity was increased to pure ethyl acetate. The product was collected as a bright pink band. Yield: 82 mg (78 %). ^{1}H NMR (400 MHz, $CDCl_3$) δ 9.400 (*dd*, J_A = 4.4 Hz, J_B = 2.4 Hz, 2H, pyrrole H), 8.973 (*dd*, J_A = 4.8 Hz, J_B = 4.0 Hz, 2H, pyrrole H), 8.934 (*dd*, J_A = 4.0 Hz, J_B = 3.6 Hz, 2H, pyrrole H), 8.810 (*dd*, J_A = 4.8 Hz, J_B = 2.8 Hz, 2H, pyrrole H). ^{19}F NMR (400 MHz, $CDCl_3$) δ -136.37 (*m*, 6F, 2,6-phenyl F), -151.53 (*t*, *J* = 24 Hz, 2F, 4-phenyl F), -151.77 (*t*, *J* = 20 Hz, 1F, 4-phenyl F), -161.01 (*td*, J_A = 20 Hz, J_B = 8 Hz, 4F, 3,5-phenyl F), -161.21 (*td*, J_A = 20 Hz, J_B = 4 Hz, 2F, 3,5-phenyl F).

Chapter 3

DEVELOPMENT OF THE *BIS*(IMINO)DIPYRROMETHANE LIGAND

3.1 Background

Development of redox non-innocent ligands have been of interest for in the search of new catalysts. As mentioned above, the development of the phlorin ligand was initial to infuse the redox non-innocence into porphyrinoid macrocycles.[15-17] This was done by incorporating sp^3-hybridized *meso* carbons into the structure. This is inspired by the redox non-innocence of the porphyrinogen macrocycle, another tetrapyrrole macrocycle with four sp^3-hybridized macrocycles.[18-20] Another field in the development of these redox non-innocent ligands has been the development of *bis*(imino) ligands.[36]

3.1.1 *Bis*(imino) Ligands

The *bis*(imino) moity has been explored in the development of redox non-innocent ligands for its ability to both accept and donate electron-density to a coordinated metal center.[36] Initial reports of ligands utilizing this moity utilized a pyridyl spacer, yielding a tridentate ligand.[37,38] These *bis*(imino)pyridine ligands were used in combination with late-transition metals to develop catalysts for ethylene polymerization.[39] This work has been championed using iron and cobalt as the metal center. Because of this ligands ability to both accept and donate electron-density, the ligand was able to influence the redox potential of the coordinated metal center. While initial work has been done on transition metal catalyst, another field of study

has explored the effect of this class of ligand on lanthanides and main group metal centers.

3.1.2 Work from the Chirik Group

The Chirik group has begun investigating the *bis*(imino)pyridine iron complexes as a catalyst for small molecule activation and transformations. Initial studies of the compounds showed an ability to activate dinitrogen.[40] Later studies published by the Chirik group showed that *bis*(imino) ligand catalysts were able to support hydroborylations[41,42] and carbon-carbon bond forming reactions.[43] These studies serve as evidence that these non-innocent redox ligands have applications outside of their traditional field of polymerization catalysis.

3.1.3 Investigation of Other *Bis*(imino) Spacers

While the *bis*(imino) moity has been widely studied on the pyridyl spacer, there have been studies done investigating other spacers.[44] These studies investigated both the donor atom in the spacer, as well as ring-size and bite angle of the spacers. 5-membered ring spaced ligands did not yield the desired complexes. This was attributed in part to the large bite angles the spacer imposed on the resultant complex. The study did overcome this by expanding the arms of the complex, but this was only effective when coupled with the anionic nitrogen donation of carbazolidyl spacer. Stronger electron donation from the spacer shows to improve the overall stability of the molecule as furan and thiophene spaced ligands did not yield the desired iron and cobalt complexes in this study.

3.1.4 Dipyrromethane Spacer

Our study investigates another potential spacer for the *bis*(imino) moity, dipyrromethane. The reasons for introducing this spacer are threefold: 1) it is a *bis*chelating spacer and will yield a tetradendate ligand, 2) it has two anionic nitrogen donors, which should stabilize metal complexes, 3) it is a redox-active moity. As previously mentioned dipyrromethane serves as a building block in the construction of the phlorin macrocycle. It is this moity that instills the multielectron redox transformations capabilities into the macrocycle[15-17] through the formation of a *spiro* propane at the sp^3-hybridized position. The combination of this multielectron redox capability with the redox facilitating imino moieties could serve to enhance catalysis.

3.2 Synthesis of *Bis*(*N*-phenyliminomethyl)dipyrromethane

The synthesis of dipyrromethane was outline above in chapter two. The final ligand was synthesized through a condensation reaction of a diacetyl functionalized dipyrromethane and aniline.

The dipyrromethane was functionalized following a procedure developed by Panda.[45] *N*,*N*-dimethylacetamide reacted with phosphorous(V) oxychloride at 0 °C for fifteen minutes. 1,2-dichloroethane diluted the resulting mixture, still at 0 °C. A solution of dipyrromethane in 1,2-dichloroethane was added dropwise to the solution. The reaction was heated to reflux for one hour. The reaction mixture then cooled and a saturated solution of sodium acetate was added dropwise. The result was a biphasic mixture. This mixture was heated at reflux for three more hours. The reaction cooled to room temperature and the product was extracted with dichloromethane. The product was washed and purified on a silica column.

The diacetyl functionalized dipyrromethane was then used to synthesize *bis*(imino) ligands. Initial attempts to develop these ligands attempted condensation with aniline using *p*-toluenesulfonic acid as an acid catalyst. These reactions lasted multiple days and failed to yield the desired product. More nucleophilic amines, such as butyl amine and cyclohexyl amine, were investigated to facilitate the condensation reaction. However these reactions failed to produce the desired compounds. The *bis*(imino) ligand was successfully synthesized through a condensation reaction with a stronger lewis acid catalyst, titanium(IV) chloride.

The synthesis of *Bis*(*N*-phenyliminomethyl)dipyrromethane was developed based on a procedure by Novak.[46] A solution of titanium(IV) chloride in toluene was added to a solution of aniline in toluene. The solution was heated at 90 °C for ten minutes. A suspension of the diacetyl dipyrromethane in toluene was added to the reaction dropwise. The reaction was heated at 90 °C for one day. The reaction was cooled to room temperature and dichloromethane was added to dissolve residual solid. The mixture was washed and purified on a silica column.

3.3 Metalation of *Bis*(*N*-phenyliminomethyl)dipyrromethane

3.3.1 Metalation of Zinc

Metalation of the ligand with zinc were initially attempted using zinc(II) acetate in *N*,*N*-dimethylformamide at reflux. This reaction did not yield the desired product; the free-base ligand was recovered from the reaction. It was determined that the acetate was not basic enough to deprotonate the ligand to enable metalation. Successful metalation was achieved using diethyl zinc.

The reaction of *bis*(*N*-phenyliminomethyl)dipyrromethane with diethyl zinc was performed in a moisture-free nitrogen glovebox. The ligand was dissolved in toluene, and a solution diethyl zinc in hexanes was added to the solution dropwise. The compounds reacted at -36 °C for one day. Unreacted diethyl zinc was quenched with methanol. The reaction was filtered and the solvent was stripped. The residue was washed with chilled hexanes to yield the desired product.

The ^{1}H NMR showed the peaks had shifted from their resonances in the free-base spectrum. The high-resolution mass spectrum showed a peak corresponding to a dimeric complex. This dimeric complex was confirmed by the solid-state crystal structure.

3.3.1.1 Crystal Structure of Zinc Complex

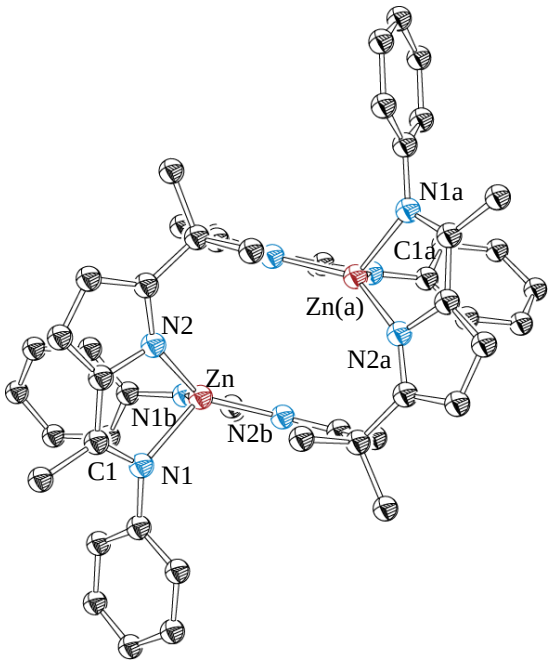

Figure **21**. Thermal ellipsoid plot of [Zn(BIDPM)]$_2$ with ellipsoids drawn at 50 % probability level. Hydrogen atoms omitted for clarity.

3.3.1.1.1 Bonding Metrics of Interest

[Zn(BIDPM)]$_2$ (Figure 21): Selected bond lengths (Å) and angles (°): C1-N1 1.310 ± 0.005, N1-Zn 2.066 ± 0.007, N2-Zn 1.978 ± 0.007, N1-Zn-N2 83.6 ± 0.4, N1-Zn-N1b 106 ± 4, N2-Zn-N2b 141 ± 2,N1-Zn-N2b 121 ± 2.

3.3.2 Metalation of Nickel

Nickel(II) acetate•tetrahydrate was dissolved in *N,N*-dimethylformamide. A solution of the ligand in *N,N*-dimethylformamide was added to the flask via syringe. The reaction was heated at 90 °C for eighteen hours. The reaction solvent was stripped, and the residue was dissolved in dichloromethane. The solution was washed and concentrated. The residue was then dissolved in acetonitrile and filtered. The solvent was stripped to isolate the product. The product was confirmed by its ^{1}H NMR spectrum and high-resolution mass spectrum. This product was isolated as a monomer, which was confirmed by a solid-state crystal structure.

3.3.2.1 Crystal Structure of Ni(BIDPM)

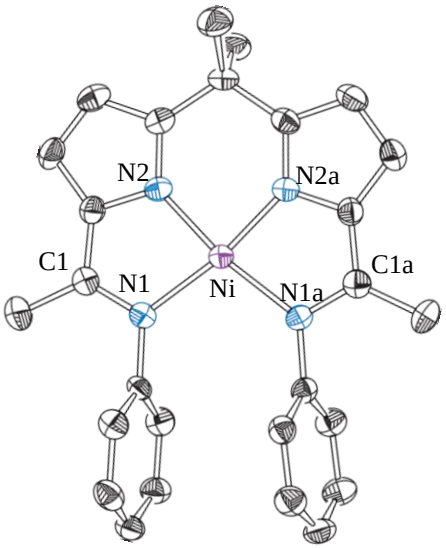

Figure **22**. Thermal ellipsoid plot of Ni(BIDPM) with ellipsoids drawn at 50 % probability level. Hydrogen atoms omitted for clarity.

3.3.2.1.1 Bonding Metrics of Interest

Ni(BIDPM) (Figure 22): Selected bond lengths (Å) and angles (°): N1-C1 1.327 ± 0.001, Ni-N1 1.965 ± 0.003, Ni-N2 1.837 ± 0.003, N1-Ni-N2 83.27, N2-Ni-N2a 87.54, N1a-Ni-N2a 83.31, N1-Ni-N1a 105.87.

3.4 Electronic Spectroscopy of Compounds

3.4.1 Free-Base *Bis*(*N*-phenyliminomethyl)dipyrromethane

The electronic spectrum of the free-base ligand was acquired in several solvents: dichloromethane, acetone, acetonitrile, benzene, tetrahyrdofuran, and *N*,*N*-dimethylformamide. Across different solvents the features of the spectrum remained consistent. A representative spectrum from this series in dichloromethane is shown

below (figure **23**). This spectrum features one sharp peak, centered at 299.5 nm with a molar absorptivity of 66,700 $M^{-1}cm^{-1}$. The maxima of this peak shifted depending on the solvent from which the spectrum was obtained. This effect is represented below in solvatochroism plot, which plots wavelength of peak versus the dielectric constant of the solvent (figure **24**). The plot show does not show a linear trend between maxima wavelength and dielectric constant, which would indicate a polar excited state. The maxima in acetone shows the biggest variance from the other maxima. This may correlate to the increased acidity of acetone relative to the other solvents.

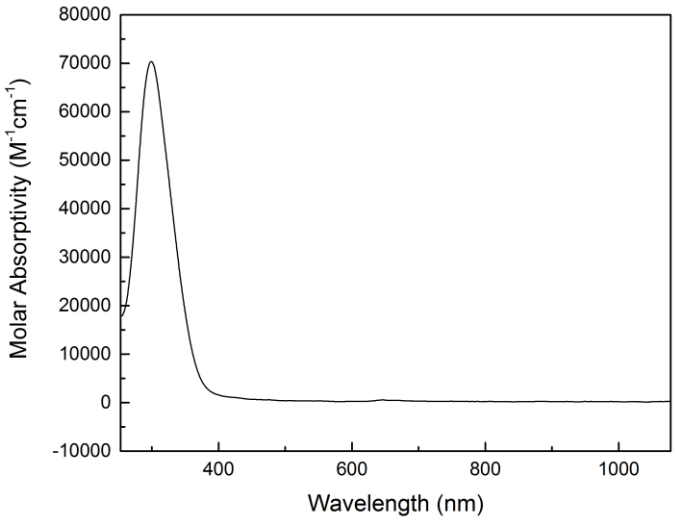

Figure **23**. Electronic Spectrum of *Bis*(*N*-phenyliminomethyl)dipyrromethane.

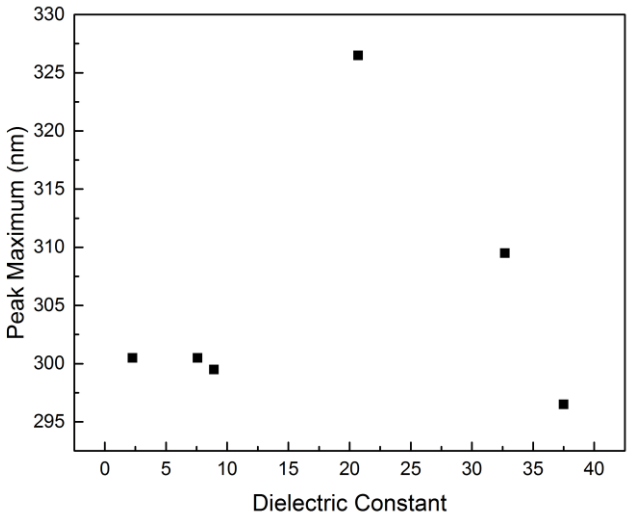

Figure **24**. Solvatochroism plot of *bis*(*N*-phenyliminomethyl)dipyrromethane.

3.4.2 [Zn(BIDPM)]$_2$

The electronic spectrum of the zinc complex was also obtained in several solvents: dichloromethane, acetone, benzene, tetrahyrdofuran, and *N*,*N*-dimethylformamide. A representative spectrum in dichloromethane is shown below (figure **25**). This spectrum features one sharp peak like the free-base spectrum. The peak maxima was red-shifted to 361 nm, and the molar absorptivity (relative to ligand equivalences) was 39,600 $M^{-1}cm^{-1}$. The solvatochroism plot (figure **26**) shows a trend where the more polar solvents experience a blue-shift. The dichloromethane does not follow this trend and is shifted blue more so than the more polar solvents.

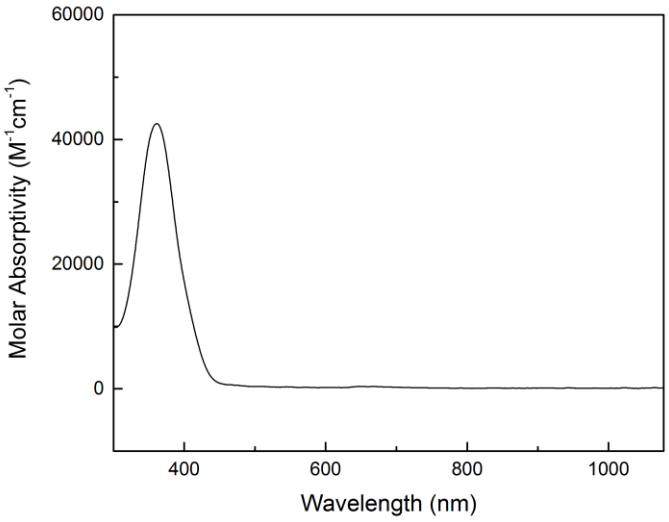

Figure **25**. Electronic Spectrum of $[Zn(BIDPM)]_2$.

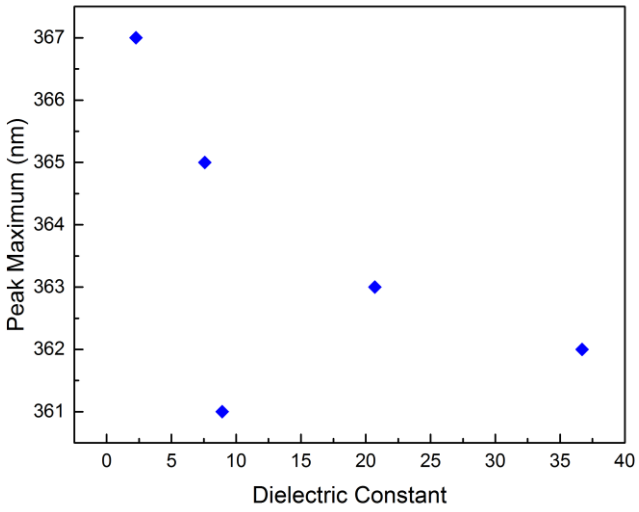

Figure **26**. Solvatochroism plot of $[Zn(BIDPM)]_2$.

3.4.3 Ni(BIDPM)

The electronic spectrum of the nickel complex was obtained from a dichloromethane solution (figure **27**). The spectrum showed three features. There is a sharp feature that correlates to the feature seen in the free-base and zinc complex. This peak has been red-shifted from the free-base spectrum to 325 nm. The molar absorptivity has also been attenuated from the free-base to 24,700 $M^{-1}cm^{-1}$. The two other features are shoulders at lower energies to this peak. The shoulder at 363 nm had a molar absorptivity of 8630 $M^{-1}cm^{-1}$. The other shoulder, at 427 nm, had a molar absorptivity of 7080 $M^{-1}cm^{-1}$. These additional features are attributed to charge-transfers between from ligand to metal. These were not observed in the zinc complex because zinc(II) has no unoccupied *d* orbitals to receive charge from the ligand.

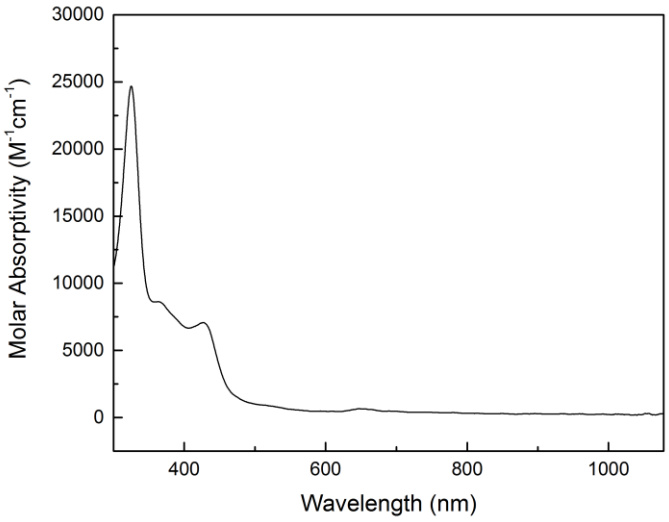

Figure **27**. Electronic Spectrum of Ni(BIDPM).

3.4.4 Comparison of Spectra

Across the three spectra, the most intense absorptions are observed in the free-base ligand. In both metal complexes an attenuation of their absorption features is observed. This attenuation is more pronounced in the nickel complex, which might be due to this complexes capacity for charge transfer. The principle feature of metal complexes also experienced a red-shift relative to the free-base ligand. This suggests a lowering of the HOMO-LUMO gap of the ligand when bound to a metal center. This suggests that there is a degree of orbital mixing within the complexes shrinking the gap. This result is consistent with the thesis of the ligands design, suggesting an interaction of the *bis*(imino) moity's orbitals and the metal orbitals.

3.5 Electrochemical Studies

3.5.1 Zinc Complex

By analyzing this ligand while bound to a zinc(II) nucleus we expect to observe only ligand-centric redox events. Because the third principle energy level of zinc(II) is filled, and the fourth energy level does not contain any electrons, this nucleus is resistant to both oxidative and reductive events. The zinc complex was study as opposed to the free-base in the hopes that the zinc complex would provide a more stable analyte upon oxidation and reduction.

3.5.1.1 Cyclic Voltammetry

The cyclic voltammagrams were obtained from a solution of *N*,*N*-dimethylformamide using a platinum working electrode, platinum counterelectrode, and silver wire working electrode (figure **28**). Decamethylferrocene was used as an internal standard. The most negative wave of the anodic scan was at 0.9 V vs.

Fc^*/Fc^{*+}. There was also another less defined current response more positive of this feature, possibly due to the decomposition of the complex. The cathodic scan featured a response at -2.2 V vs. Fc^*/Fc^{*+}. This feature appears to be composed of two reductions with less than 100 mV of separation. This suggests that the compound experiences a small degree of electron delocalization. This event could be characterized as a class II under the Robin-Day classification criteria. Because of the dimeric nature of this compound however it is difficult to ascertain whether the difference is due to communication between the separate ligands through the zinc center or between the two halves of the same ligand through the quaternary carbon link between the pyrrole subunits.

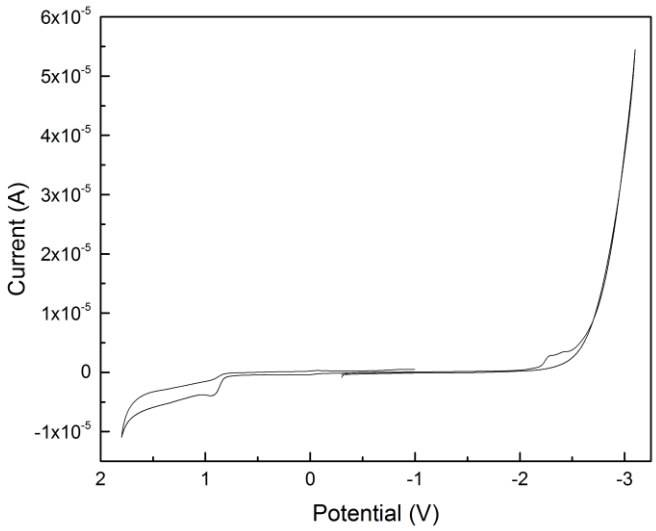

Figure **28**. Cyclic Voltammagrams of $[Zn(BIDPM)]_2$.

3.5.1.2 Differential Pulse Voltammetry

The differential pulse voltammagrams of the complex were obtained from a solution of *N*,*N*-dimethylformamide using a platinum working electrode, platinum counter electrode, and a silver wire reference electrode (figure **29**). Decamethylferrocene was used as an internal reference for the scans. These scans were consistent with the cyclic voltammagrams of this compound. The anodic scan had a peak at 0.9 V vs. Fc^*/Fc^{*+} and the cathodic scan had a peak at -2.2 V. There was a current response prior to the foot of the -2.2 V peak. This is possibly caused by surface interaction of the complex with the working electrode. Unlike the cyclic voltammagram, the -2.2 V peak did not have a double feature. The areas of the two peaks equal in area with one another

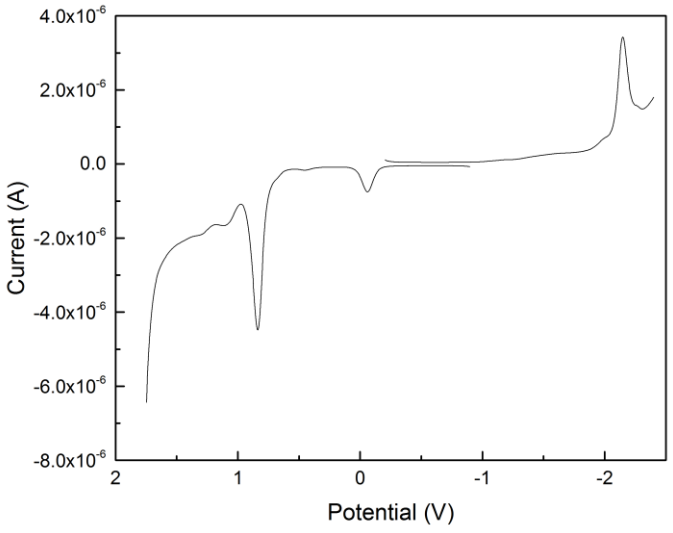

Figure **29**. Differential Pulse Voltammagram of $[Zn(BIDPM)]_2$.

3.5.2 Nickel Complex

These electrochemical studies aimed to investigate the interplay between the ligand orbitals and the redox-active metal center of nickel(II). By comparing these result with those obtained from the zinc(II) complex, we hope to infer the characteristics of the metal and ligand orbitals interaction.

3.5.2.1 Cyclic Voltammetry

Cyclic voltammagrams of Ni(BIDPM) were taken in *N*,*N*-dimethylformamide with a platinum working electrode, platinum counterelectrode, and silver wire reference electrode at various scan rates. The scans were referenced with an internal standard of decamethylferrocene. The scans showed below were record at a scan rate of 10 mV/s (figure **30**). The cathodic scan contained a large wave at -2.6 V vs. Fc^*/Fc^{*+} that was not reversible. This feature was more pronounced than the wave observed in the voltammagram of the zinc complex. However the scan of the nickel complex had a larger current response. In the anodic scan of the complex there was one minute feature at 0.5 V vs. Fc^*/Fc^{*+}. This feature was quasireversible at the 10 mV/s scan rate. Compared to the cathodic response at -2.6 V this response was significantly smaller. This response was also more positive of responses observed in the zinc complex.

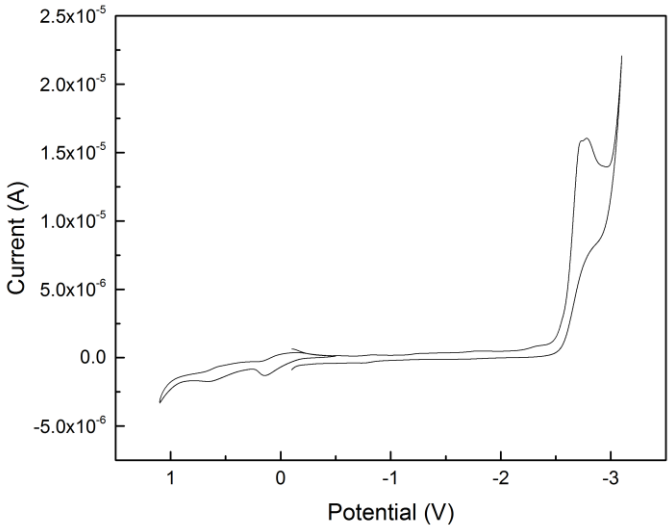

Figure **30**. Cyclic Voltammagram of Ni(BIDPM).

3.5.2.2 Differential Pulse Voltammetry

The differential pulse voltammagrams of Ni(BIDPM) were taken in a solution of *N*,*N*-dimethylfomamide using a platinum working electrode, platinum counterelectrode, and silver wire reference electrode (figure **31**). The scans were referenced with a decamethylferrocene internal standard. These scans agreed with the features observed in the cyclic voltammagram. The cathodic scan showed a large peak at -1.6 V vs. Fc^*/Fc^{*+}, and the anodic scan showed a small feature at 0.5 V vs. Fc^*/Fc^{*+}. The areas of the peaks showed that the cathodic peak was approximately four times as large as the anodic peak. A four electron redox event is exceedingly rare, which suggests that the event at -2.6 V is a coalescence of two two-electron reductions.

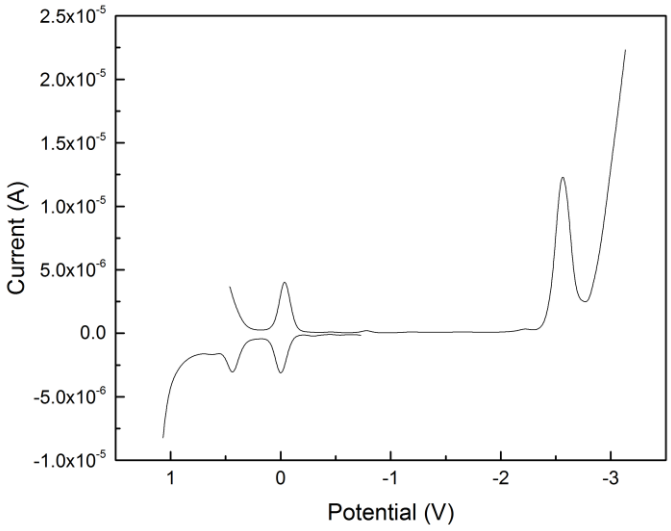

Figure **31**. Differential Pulse Voltammagram of Ni(BIDPM).

3.6 Summary

This study explored the characteristics of a new ligand which utilizes the *bis*(imino) moiety to facilitate redox transformations. In this study the ligand was synthesized and characterized with NMR spectroscopy and electronic spectroscopy. The ligand was then metalated with zinc(II) and nickel(II), and their strctures were confirmed using X-ray diffraction crystallography. In addition the reduction and oxidation potentials of these compounds were probed using cyclic voltammetry and differential pulse voltammetry.

Zinc(II) being a d^{10} metal, is most stable in a tetrahedral geometry. The flexibility of ligand granted by its tetrahedral carbon linker allowed this geometry to be achieved through the formation of a dimer species. The dimer was confirmed through its LIFDI mass spectrum and crystal structure. The crystal structure showed the zinc centers took a distorted tetrahedral geometry. The ^{1}H NMR spectrum shows

that this complex maintains its symmetry. Additionally from the crystal structure, the distance between zinc nuclei is 4.340 Å, too far for an intermetallic bond. While the zinc(II) metal is inherently stable oxidation state, the flexibility that this ligand shows to permit the formation of a dimeric species could be of interest to other metal centers, perhaps even allowing the formation of intermetallic bonds with in the nuclei. Additionally connecting two redox-active metal centers would enable a study of the ligands own capacity for electron-delocalization as a whole, using the Robin-Day classification.

The metalation with nickel(II) yield a monomeric complex, displaying this ligands capacity to form monomers or dimers, depending on the metal centers steric demands. The nickel(II) complex was completely planar around the metal center with bond angles distorted from a true square planar geometry.

This ligand shows promise due to its flexibility and capacity to form bimetallic complexes. Future studies should expand on these preliminary metalations, expanding the library of metal complex to gain more insight as to what governs the formation of a monomer versus a dimer. Additionally, the synthesis of the *bis*(imino) ligand was proven challenging, due to solubility issues with the diacetyl starting material. Replacing the acetyl groups with another acyl group may facilitate the transformation. *R* groups such as pentafluorophenyl could be explored as the synthesis of this material is known and outline in a previous chapter. Furthermore these could provide a means to tune the electronics of compounds of interest.

Bimetallic constructs can be seen throughout nature, particularly in energy-relevant pathways. This ligand provides as synthetically simple framework to achieve a bimetallic complex. While this study has shown the ligands capacity for the

formation of a dimeric complex with a metal center that prefers a tetrahedral geometry and a monomeric complex with a metal center that prefers square planar geometry, how the ligand adapts two a nuclei that prefers five coordinate geometries, like iron(III), would be interesting, particularly if it leads to dimer containing a metallic bond. Additionally developing a method creating a heterometallic complex could yield interesting reactivity. Ultimately this study led to creation of a new ligand that is geometrically flexible, but more work must be done to determine this ligand full capabilities and potential applications.

3.7 Experimental

3.7.1 General Synthetic Methods:

Reactions were carried out under open air unless otherwise specified. Reactants and solvents were obtained from Sigma-Aldrich, Fisher, Strem, Acros, or Cambridge Isotopes Laboratories. Chemicals were used as obtained unless otherwise specified.

3.7.2 Spectroscopic Methods:

NMR spectra were obtained at room temperature. Proton and carbon spectra were obtained referenced to residual deuterated solvent peaks (^{1}H: CD_3CN, $\delta = 1.94$; $CDCl_3$, $\delta = 7.26$; ^{12}C: CD_3CN, $\delta = 1.32, 118.26$; $CDCl_3$, $\delta = 77.16$). All chemical shifts are reported with standard δ notation in parts-per-million.

UV/visible spectra were obtained at room temperature on a StellarNet CCD array UV-vis spectrometer using quartz cuvettes with pathlength of 1 cm. Spectra were obtained at room temperature.

Electrochemical studies were preformed using a CHI-620D potentiostat/galvanostat. Cyclic voltammetry (CV) and differential pulse voltammetry (DPV) were performed in a nitrogen glovebox with a three electrode set-up. CV and DPV scans were recorded with a glassy carbon working electrode, a platinum wire counterelectrode, and a silver wire quasi-reference electrode. Experiments were performed with 0.1 M solution of tetrabutylammonium hexafluorophosphate in either acetonitrile or dichloromethane. Potentials were referenced to standard hydrogen electrode using an internal standard of decamethylferrocene.

3.7.3 Synthesis of 2,2'-*Bis*(acetyl)-5,5-Dimethyldipyrromethane

A three-neck flask was set-up with a condenser, addition funnel, and a septa. Dimethyl acetamide (3 mL, 68 mmol) was added to the flask and cooled in an ice bath. Phosphorous oxychloride was added dropwise via addition funnel. The reaction was stirred for fifteen minutes at room temperature. Dichloroethane (10 mL) was added to the reaction mixture. The mixture was cooled in an ice bath. A solution of 5,5-dimethyldipyrromethane (1.016 g, mol) in dichloroethane (10 mL). The reaction was heated to reflux for one hour. A saturated solution of sodium acetate (12 g) in water was added slowly via the addition funnel. The biphasic mixture was heated at reflux for three hours. The reaction was extracted three times with dichloromethane. The organic layer was washed with a solution of sodium carbonate then dried over sodium sulfate. The solution was removed *in vacuo*. The product was isolated off a silica column with a 7:3 mixture of hexane and ethyl acetate eluent. Yield: 1.050 g (71

%). ^{1}H NMR (400 MHz, $CDCl_3$) δ 10.092 (*s*, 2H, H-N), 6.762 (*dd*, J_A = 3.6 Hz, J_B = 2.6 Hz, 2H, 4-pyrrole H), 6.094 (*dd*, J_A = 3.6, J_B = 2.9, 2H, 3-pyrrole H), 2.333 (*s*, 6H, acetyl-CH_3), 1.665 (*s*, 6H, *meso*-methyl).

3.7.4 Synthesis of 2,2'-*Bis*(*N*-phenyliminomethyl)dipyrromethane (BIDPM)

Aniline (1 mL, 11 mmol) was added to a Schleck flask with toluene (5 mL). The flask was sealed with a septa and sparged with N_2 gas. A solution of titanium(IV) chloride (0.22 mL, 2 mmol) in toluene (2 mL) was added to the reaction flask. The reaction was heated to 90 °C for ten minutes. A suspension of compound **3** (262 mg, 1.01 mmol) in 2 mL of toluene was added to the reaction dropwise. The reaction was heated for 24 hours at 90 °C. The reaction cooled to room temperature. Dichloromethane was added to the reaction flask to dissolve residual solid. A concentrated solution of sodium carbonate was added. The mixture was filtered through celite. The organic phase was separated from the aqueous phase and washed with deionized water (3x). The solution was dried over sodium sulfate. The solution was concentrated *in vacuo*. The product was purified on a silica column using 5:1 mixture of hexanes and ethyl acetate as an eluent. Yield: 104 mg (26 %). ^{1}H NMR (400 MHz, $CDCl_3$) δ 7.313 (*t*, *J* = 8.0 Hz, 4H, 3,5-phenyl H), 7.058 (*t*, *J* = 7.4 Hz, 2H, 4-phenyl H), 6.754 (*d*, *J* = 7.3, 4H, 2,6-phenyl), 6.578 (*d*, *J* = 3.7 Hz, 2H, pyrrole H), 6.130 (*d*, *J* = 3.7 Hz, 2H pyrrole H), 2.072 (*s*, 6H, acetyl CH_3), 1.740 (*s*, 6H, *meso*-methyl).

3.7.5 Synthesis of Zn(BIDPM)

Synthesis was performed in an air and moisture-free nitrogen glovebox. Compound **4** was dissolved in toluene and cooled to -36 °C for one hour. A solution of diethyl zinc in hexanes was added dropwise to the chilled reaction mixture. The mixture reacted and turned green immediately and stirred for 24 hours. Unreacted diethyl zinc was quenched with methanol. The reaction mixture was removed from the nitrogen glovebox. Solvent was removed *in vacuo*. The residue was dissolved in dichloromethane and filtered through celite. The filtrate was concentrated *in vacuo*. The solid was washed with chilled hexanes. The isolated product was dried under vacuum. Yield: 45 mg (48%). ^{1}H NMR (400 MHz, $CDCl_3$) δ 7.145 (*t*, *J* = 8.0 Hz, 4H, 3,5-phenyl H), 7.026 (*t*, *J* = 7.6 Hz, 2H, 4-phenyl H), 6.772 (*d*, *J* = 3.6 Hz, 2H, pyrrole H), 6.496 (*d*, *J* = 7.6 Hz, 4H, 2,6-phenyl H), 6.326 (*d*, *J* = 3.6 Hz, 2H, pyrrole H), 2.096 (*s*, 6H, imino CH_3), 1.586 (*s*, 6H, *meso*-methyl).

3.7.6 Synthesis of Ni(BIDPM)

Nickel(II) acetate tetrahydrate (44 mg, 0.18 mmol) was dissolved in *N*,*N*-dimethylformamide (5 mL) in a Schleck flask. The flask was sparged with nitrogen gas. A solution of compound **4** (57 mg, 0.14 mmol) in *N*,*N*-dimethylformamide (2 mL). The reaction was heated to 90 °C for eighteen hours. The reaction mixture was concentrated *in vacuo*. The residue was dissolved in ethyl acetate and washed with brine (5x). The organic layer was dried over sodium sulfate. The solvent was removed *in vacuo*, and the residue was dissolved in acetonitrile. The acetonitrile

solution was filtered to remove unreacted nickel(II) acetate. The acetonitrile was removed *in vacuo*, and the residue was dissolved in dichloromethane. The dichloromethane solution was washed with brine (3x) to remove residual *N*,*N*-dimethylformamide. The organic phase was dried over sodium sulfate. The product was isolated after concentrating *in vacuo*. Yield: 30 mg (46%). ^{1}H NMR (400 MHz, $CDCl_3$) δ 7.867 (*t*, *J* = 7.4 Hz, 2H, 4-phenyl H), 6.779 (*t*, *J* = 7.6 Hz, 4H, 3,5-phenyl H), 6.746 (*d*, *J* = 3.6 Hz, 2H, pyrrole H), 6.474 (*d*, *J* = 7.6 Hz, 4H, 2,6-phenyl H), 6.181(*d*, *J* = 4.0 Hz, 2H, pyrrole H), 1.677 (*s*, 6H, imino-CH_3), 1.621 (*s*, 6H, *meso*-methyl).

REFERENCES

1. BP, 2015. BP Statistical Review of World Energy 2015-Data Workbook. http://www.bp.com/content/dam/bp/pdf/energy-economics/statistical-review-2015/bp-statistical-review-of-world-energy-2015-full-report.pdf

2. NRC, 2010. *Advancing the Science of Climate Change*. National Research Council. The National Academies Press, Washington, DC, USA.

3. IPCC, 2014: Climate Change 2014: Synthesis Report. Contribution of Working Groups I, II and III to the Fifth Assessment Report of the Intergovernmental Panel on Climate Change [Core Writing Team, R.K. Pachauri and L.A. Meyer (eds.)]. IPCC, Geneva, Switzerland, 151 pp.

4. National Oceanic and Atmospheric Administration. Trends in Atmospheric Carbon Dioxide. http://www.esrl.noaa.gov/gmd/ccgg/trends/#mlo_full (Accessed 5/1/2016).

5. Lewis, N. S.; Nocera, D. G. *Proc. Natl. Acad. Sci. U.S.A.*, **2006**, *103*, 15729-15735.

6. Dismukes, G. C. *Science*. **2001**. *292*, 447-448.

7. NREL, 2016. *Best Research-Cell Efficiencies*. http://www.nrel.gov/ncpv/images/efficiency_chart.jpg (Accessed 5/1/2016).

8. Yella, A.; Lee, H.; Tsao, H. N.; Yi, C.; Chandiran, A. K.; Nazeeruddin, M.; Diau, E. W.; Yeh, C.; Zakeeruddin, S. M.; Grätzel, M. *Science*. **2011**, *334*, 629-634.

9. Babcock, G. T.; Wikstrom, M. *Nature*. **1992**. *356*, 301-309.

10. Centi, G.; Perathoner, S. *Catal. Today.* **2009**, *148*, 191-205.

11. Kintisch, E. *Science.* **2008**, *320*, 306−308.

12. Tachibana, Y.; Vayssieres, L.; Durrant, J. R.; *Nat. Photonics.* **2012**, *6*, 511-518.

13. Bard A. J.; Fox M. A. *Acc. Chem. Res*. **1995**, *28*, 141-145.

14. Liang, X.; Mack, J.; Zheng, L.; Shen, Z.; Kobeyashi, N. *Inorg. Chem*. **2014**, *53*, 2797 - 2802.

15. Pistner, A. J.; Yap, G. P. A.; Rosenthal, J. *J. Phys. Chem. C.* **2012**, *116*, 16918-16924.

16. Pistner, A. J.; Lutterman, D. A.; Ghidiu, M. J.; Ma, Y. Rosenthal, J. *J. Am. Chem. Soc.* **2013**, *135*, 6601-6607.

17. Pistner, A. J.; Lutterman, D. A.; Ghidiu, M. J.; Walker, E.; Yap, G. P. A.; Rosenthal, J. *J. Phys. Chem. C.* **2014**, *118*, 14124-14132.

18. Bachmann, J.; Nocera, D. G. *J. Am. Chem. Soc.* **2004**, *126*, 2829-2837.

19. Bachmann, J.; Nocera, D. G. *Inorg. Chem.* **2005**, *44*, 6930-6932.

20. Bachmann, J.; Nocera, D. G. *J. Am. Chem. Soc.* **2005**, *127*, 4730-4743.

21. Pistner, Allen. "The Development Of The 5,5-Dimethylphlorin And 10,10-Dimethylbiladiene Tetrapyrrole Platforms". Ph. D., **2015**. University of Delaware.

22. Qui, T.; Eddy, J.; Rosenthal, J. *manuscript in prep.*

23. Paolesse, R.; Nardis, S.; Sagone, F.; Khoury, R. G. *J. Org. Chem.* **2001**, *66*, 550-556.

24. Gross, Z. *J. Biol. Inorg. Chem.* **2001**, *6*, 733-738.

25. Aviv, I.; Gross, Z. *Chem. Commun.* **2007**, 1987-1999.

26. Hirakawa, K.; Kawanishi, S.; Hirano, T.; Segawa, H. *J. Photochem. Photobiol. B.* **2007**, *87*, 209-217.

27. Liang, X.; Mack, J.; Zheng, L.; Shen, Z.; Kobayashi, N. *Inorg. Chem.* **2014**, *53*, 2797-2802.

28. Simkhovich, L.; Mahammed, A.; Goldberg, I.; Gross, Z. *Chem. Eur. J.* **2001**, *7*, 1041-1055.

29. Gryko, D. T.; Koszarna, B. *Org. Biomol. Chem.* **2003**, *1*, 350-357.

30. Giribabu, L.; Kandhadi, J.; Kanaparthi, R. K. *J. Fluoresc.* **2014**, *24*, 569-577.

31. Merchán, M.; Ortí, E.; Roos, B. O. *Chem. Phys. Lett.* **1994**, *226*, 27-36.

32. Gouterman, M. *J. Mol. Specstrosc.* **1961**, *6*, 138-163.

33. Nagashima, U.; Takada, T.; Ohno, K. *J. Chem. Phys.* **1986**, *85*, 4524-4529.

34. Ghosh, A.; Wondimagegn, T.; Parusel, A. B. J. *J. Am. Chem. Soc.* **2000**, *122*, 5100-5104.

35. Young, R. H.; Wehrly, K.; Martin, R. L. *J. Am. Chem. Soc.* **1971**, *93*, 5774-5779.

36. Gibson, V. C.; Redshaw, C.; Solan, G. A. *Chem. Rev.* **2007**, *107*, 1745–1776.

37. Figgins, P. E.; Busch, D. H. *J. Am. Chem. Soc*. **1959**, *82*, 820-824.

38. Alyea, E. C.; Merrel, P. H. *Inorg. Met. Org. Chem*. **1974**, *4*, 535-544.

39. Britovsek, G. J. P.; Gibson, V. C.; Hoarau, O. D.; Spitzmesser, S. K.; White, A. J. P.; Williams, D. J. *Inorg. Chem.* **2003**, *42*, 3454-3465.

40. Bart, S. C; Lobkovsky, E.; Chirik, P. J. *J. Am. Chem. Soc.* **2004**, *126*, 13794-13807.

41. Obligacion, J. V.; Chirik, P. J. *J. Am. Chem. Soc.*, **2013**, *135*, 19107-19110.

42. Obligacion, J. V.; Semproni, S. P.; Chirik, P. J. *J. Am. Chem. Soc.*, **2014**, *136*, 4133-4136.

43. Atienza, C. C. H.; Milsmann, C.; Semproni, S. P.; Turner, Z. R.; Chirik, P. J. *Inorg. Chem.* **2013**, *52*, 5403-5417.

44. Britovsek, G. J. P.; Gibson, V. C.; Hoarau, O. D.; Spitzmesser, S. K.; White, A. J. P.; Williams, D. J. *Inorg. Chem.* **2003**, *42*, 3454-3465.

45. Mahanta, S. P.; Kumar, B. S.; Baskaran, S.; Sivasankar, C.; Panda, P. K. *Org. Lett.* **2012**, *14*, 548-551.

46. Tian, G.; Boone, H. W.; Novak, B. M. *Macromolecules*, **2001**, *34*, 7656-7663.

Appendix

EXPERIMENTAL DATA

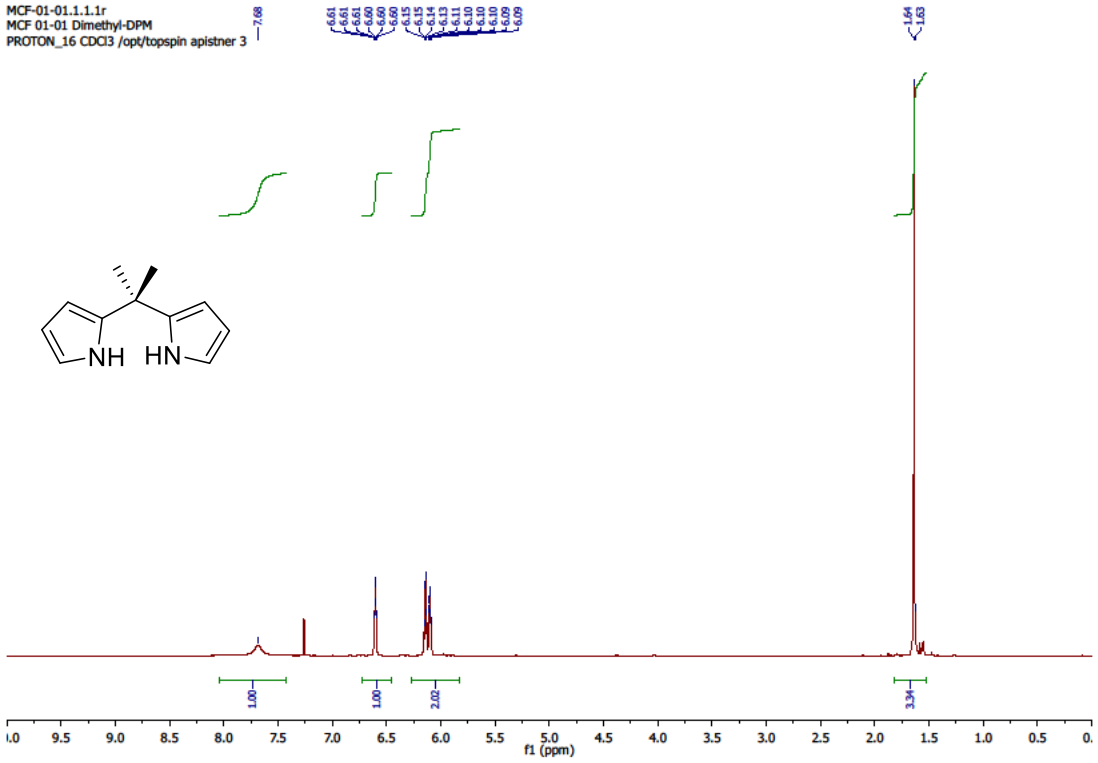

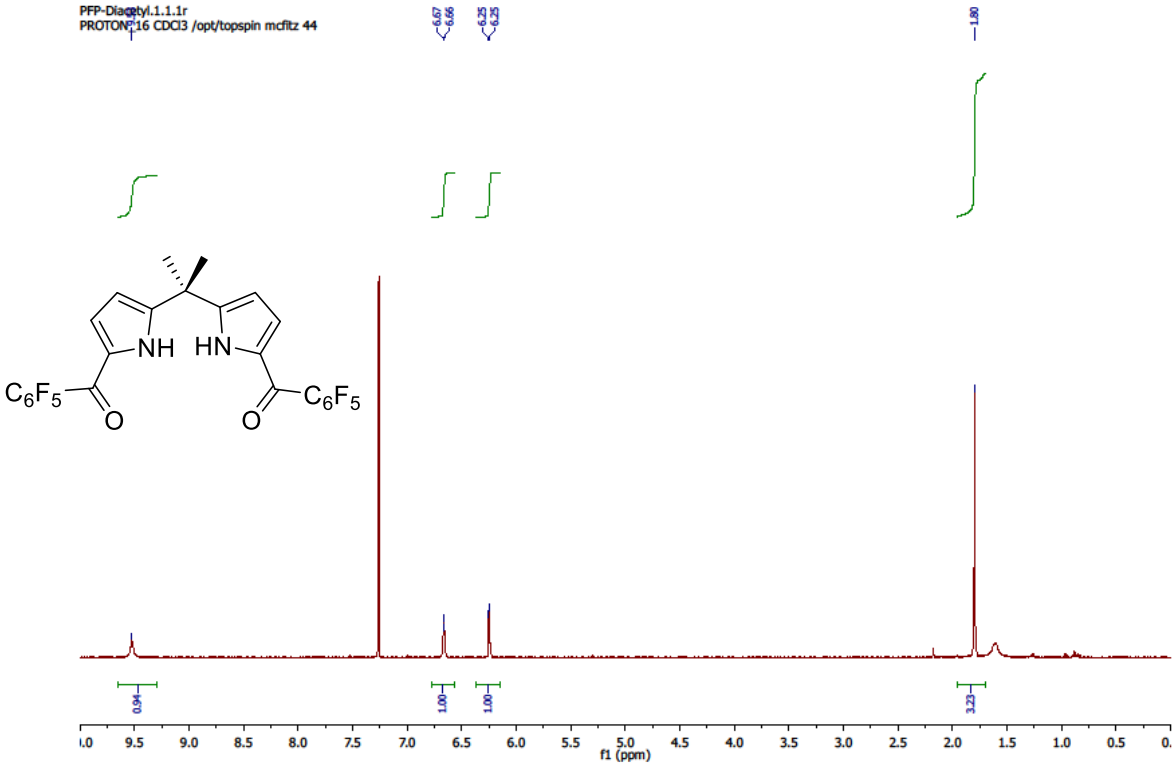
PFP-Diacetyl.1.1.1r
PROTON_16 CDCl3 /opt/topspin mcfitz 44
6.67
6.66
6.25
6.25
1.80
NH
HN
C6F5
C6F5
O
O
0.94
1.00
1.00
3.23
f1 (ppm)

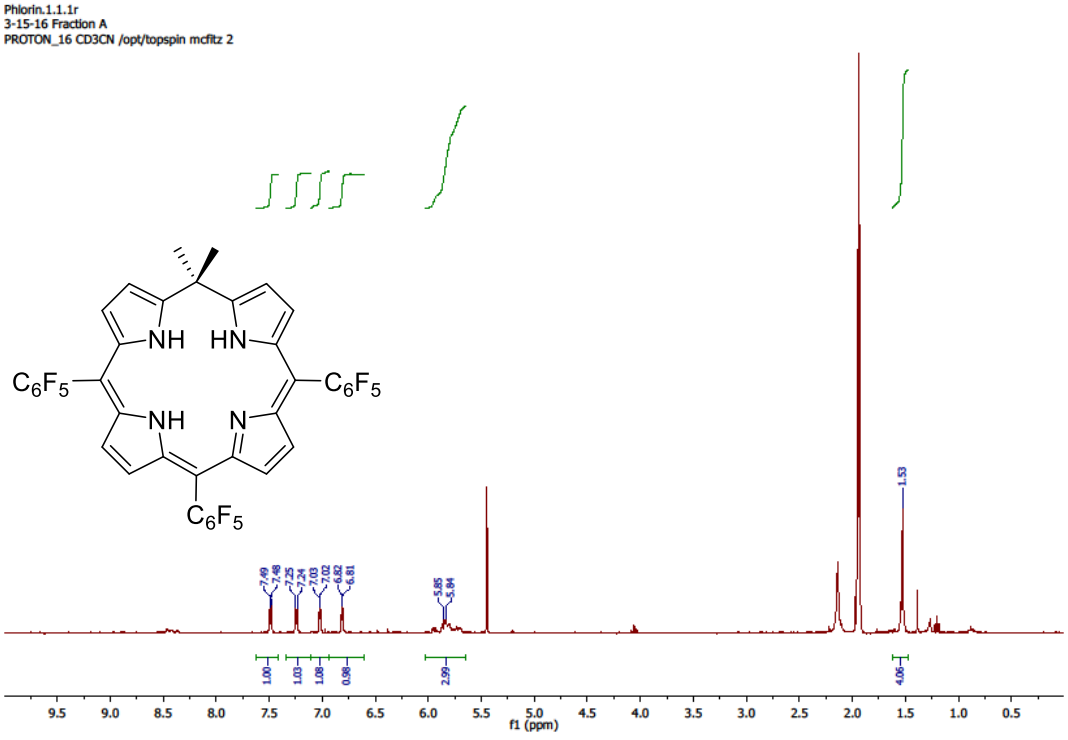
Phlorin.1.1.1r
3-15-16 Fraction A
PROTON_16 CD3CN /opt/topspin mcfitz 2
NH
HN
NH
N
C6F5
C6F5
C6F5
7.49
7.48
7.25
7.24
7.03
7.02
6.82
6.81
5.85
5.84
1.53
1.00
1.03
1.08
0.38
2.99
4.06
f1 (ppm)

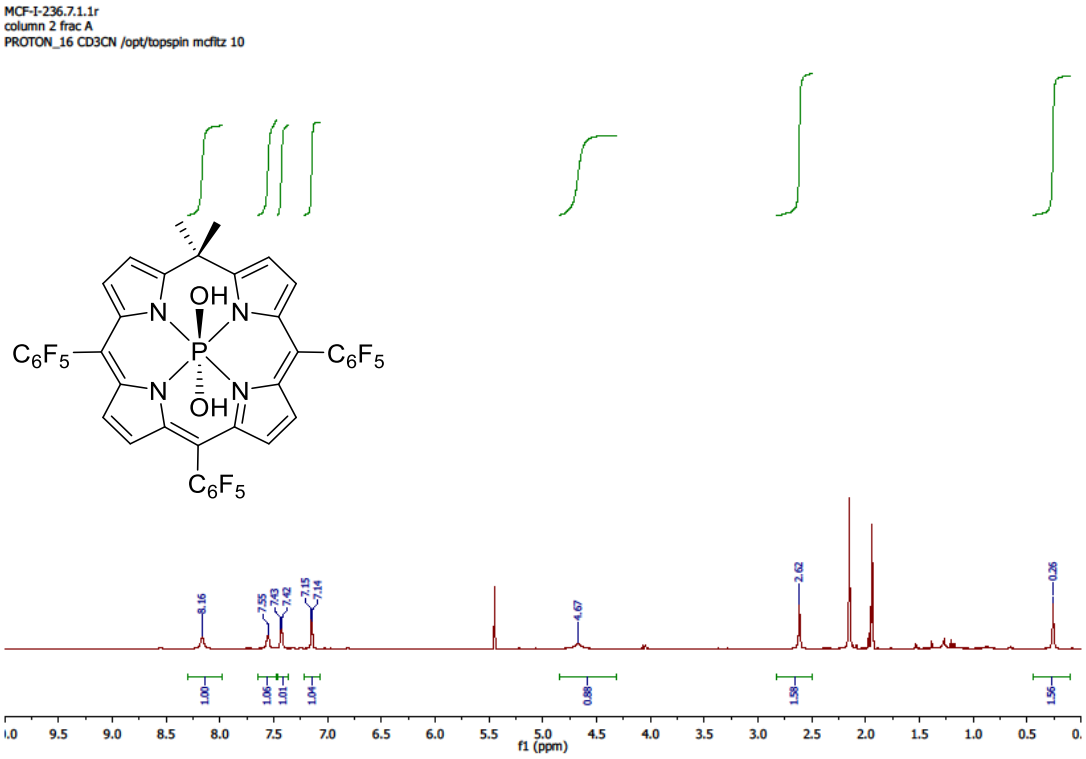
MCF-I-236.7.1.1r
column 2 frac A
PROTON_16 CD3CN /opt/topspin mcfitz 10
OH
OH
C6F5
C6F5
C6F5
8.16
7.55
7.43
7.42
7.15
7.14
4.67
2.62
0.26
1.00
1.06
1.01
1.04
0.88
1.58
1.56
f1 (ppm)

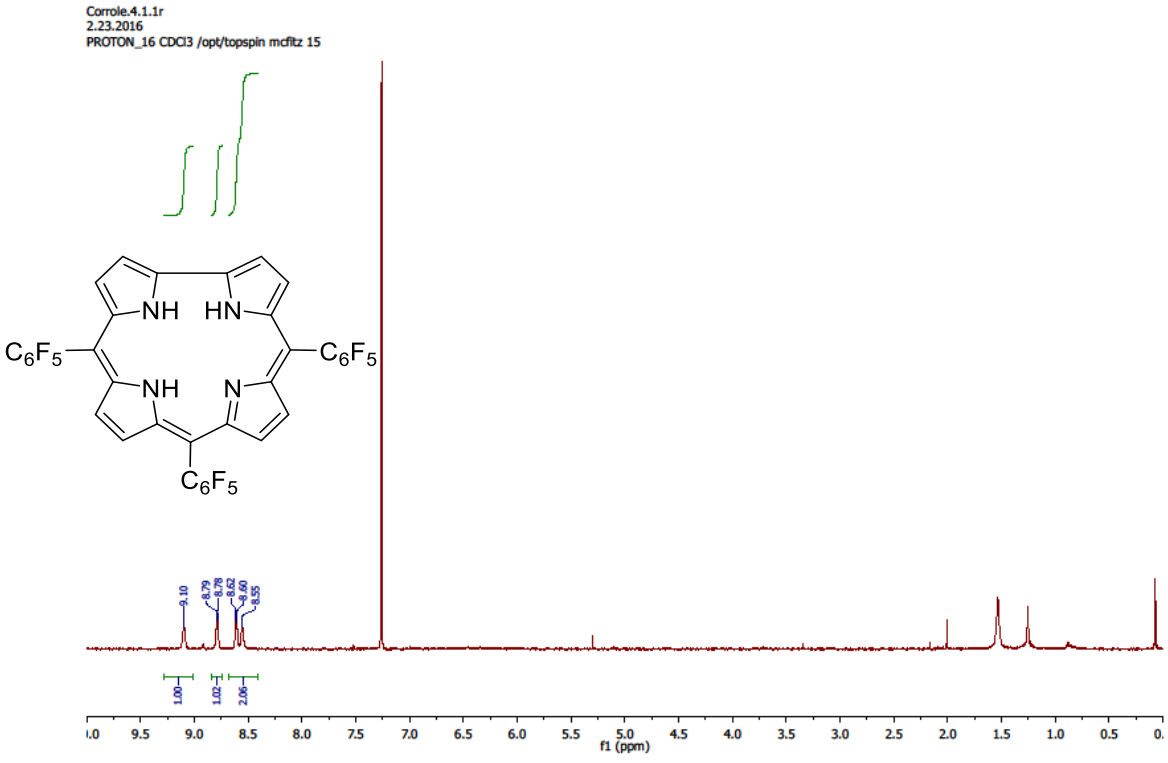
Corrole.4.1.1r
2.23.2016
PROTON_16 CDCl3 /opt/topspin mcfitz 15
NH
HN
NH
N
C6F5
C6F5
C6F5
9.10
8.79
8.78
8.62
8.60
8.55
1.00
1.02
2.06
f1 (ppm)

MCF-II-130.1.1.1r
Phosphorous Corrole
PROTON_16 CDCl3 /opt/topspin mcfitz 46

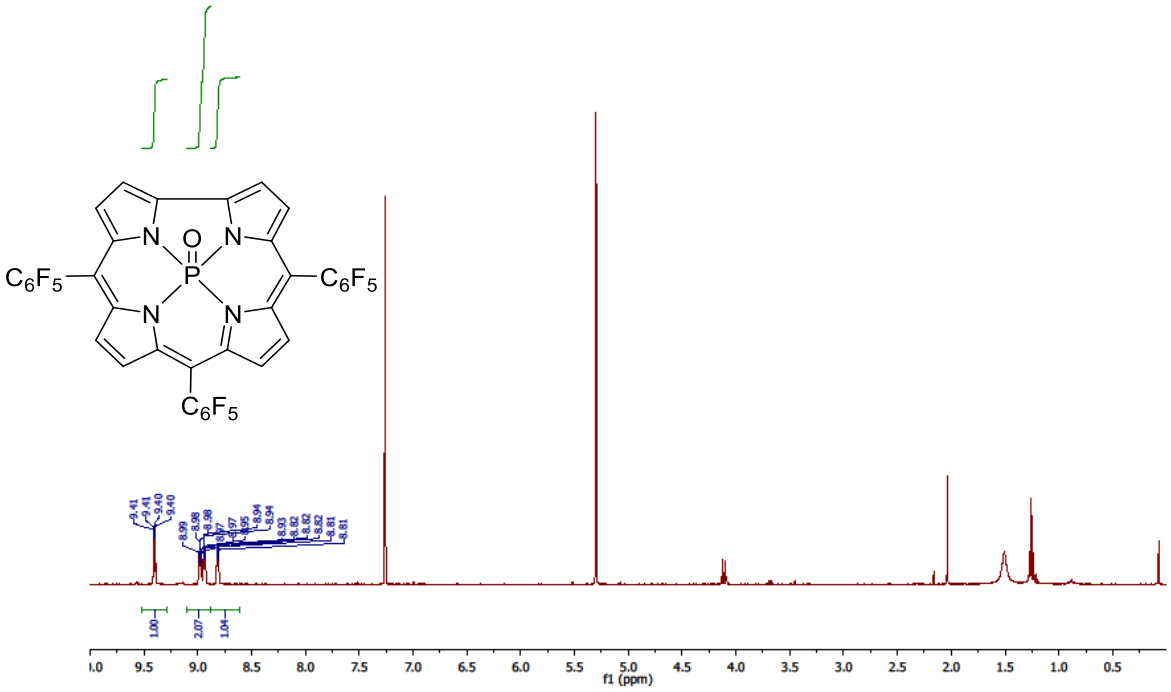

MCF-01-003.1.1.1r
MCF 01-003 Methyl-Diacyl
PROTON_16 CDCl3 /opt/topspin apistner 25

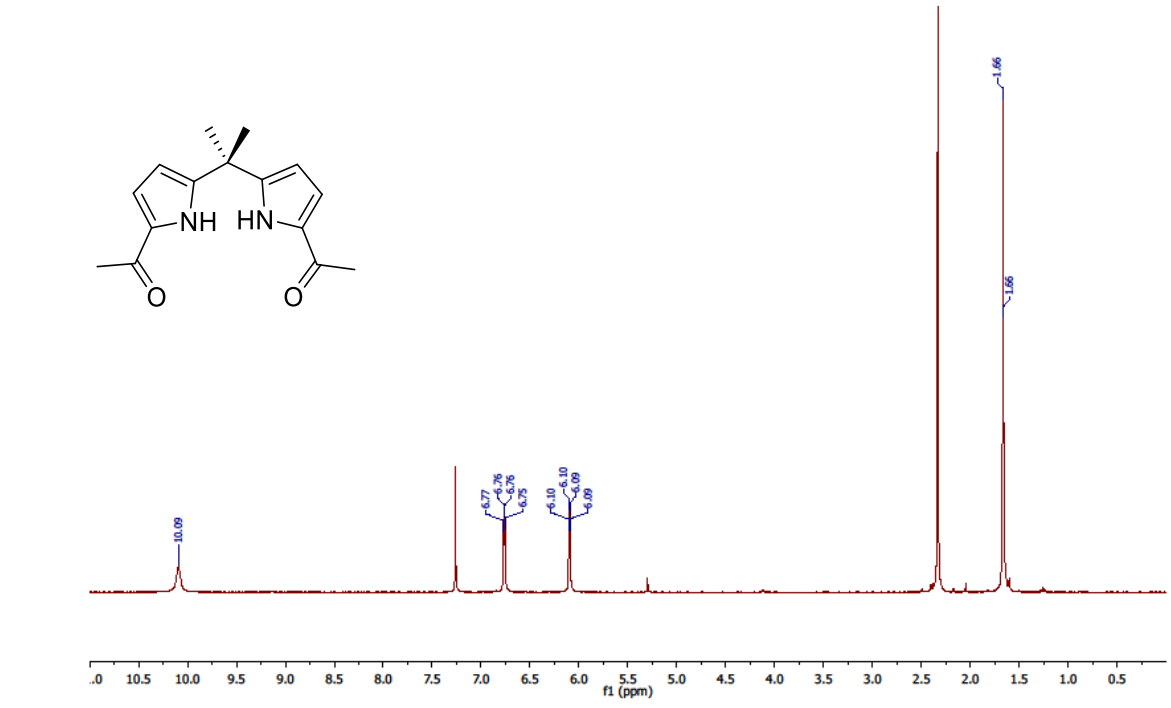

MCF-I-073.6.1.1r
After cold pentane wash
PROTON_16 CDCl3 /opt/topspin mcfitz 31

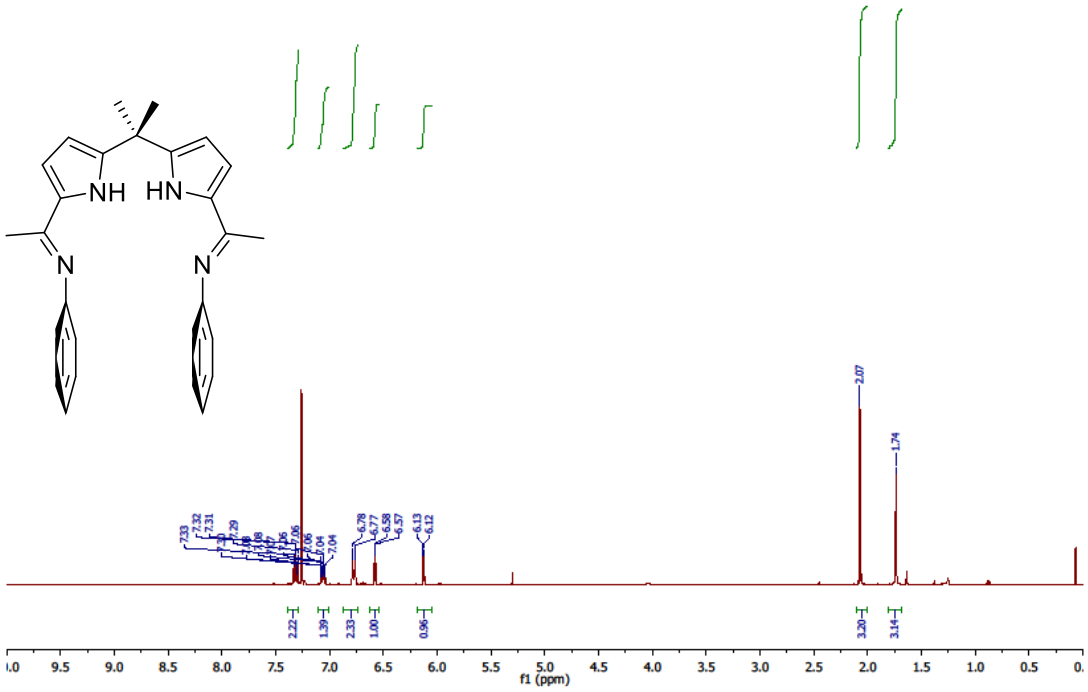

MCF-I-097.3.1.1r
Hexane solid
PROTON_16 CDCl3 /opt/topspin mcfitz 28

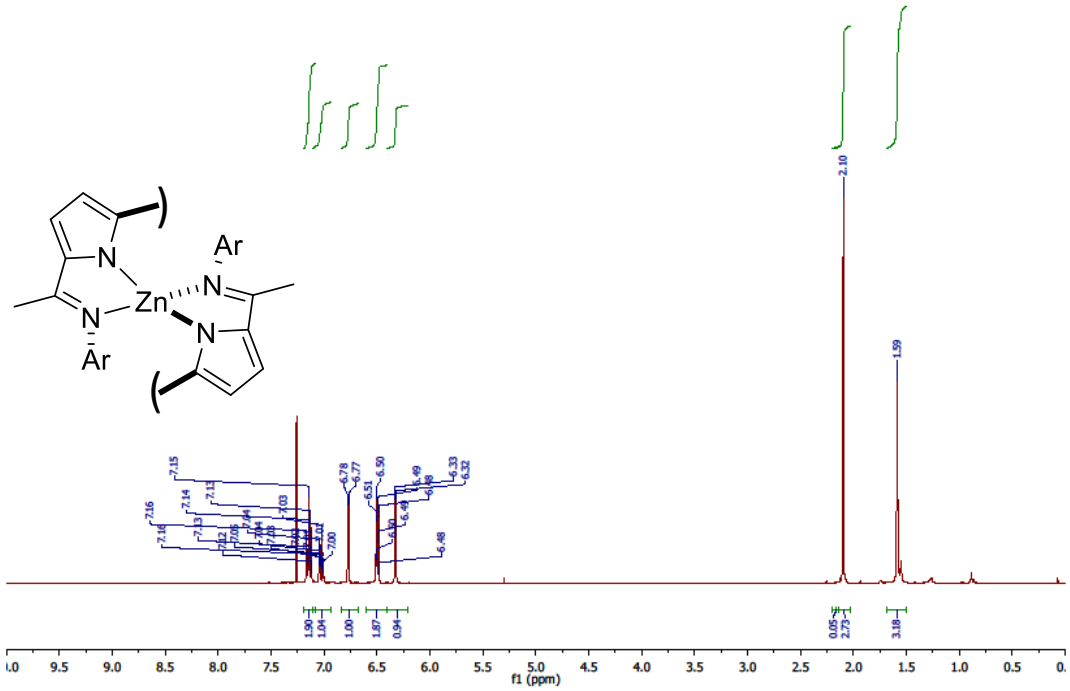

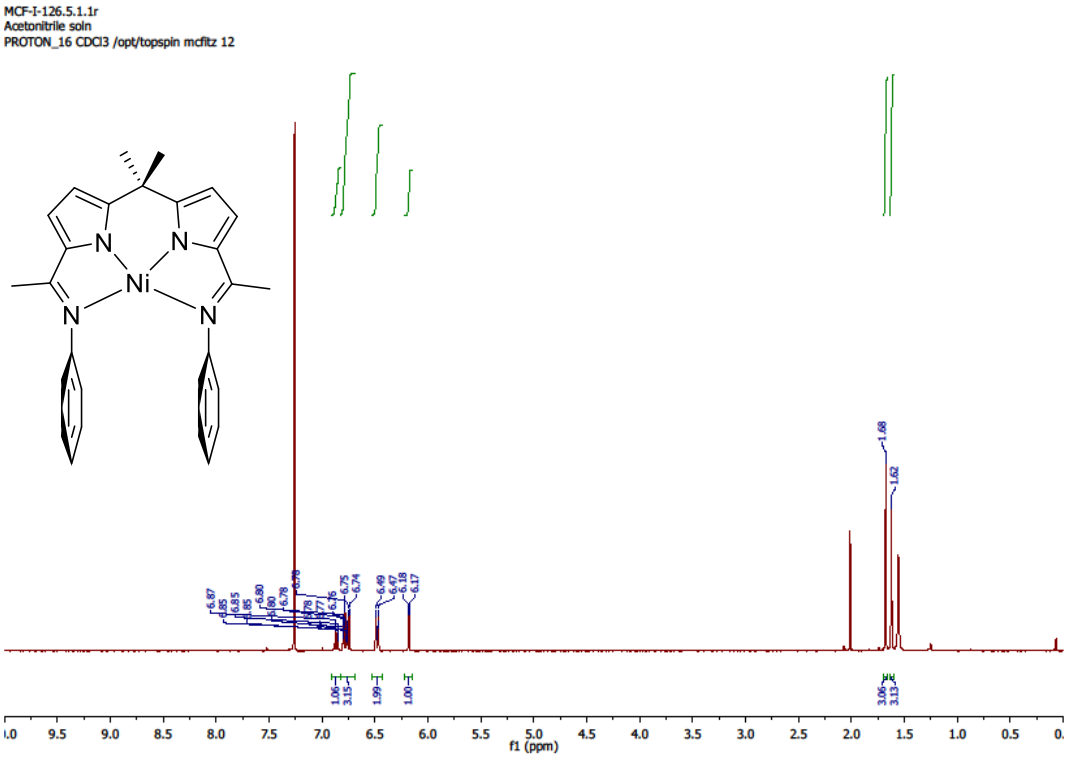
MCF-I-126.5.1.1r
Acetonitrile soln
PROTON_16 CDCl3 /opt/topspin mcfitz 12
N
N
Ni
N
N
1.68
1.62
6.87
6.85
6.85
6.80
6.80
6.78
6.78
6.78
6.77
6.76
6.75
6.74
6.49
6.47
6.18
6.17
1.06
3.15
1.99
1.00
3.05
3.13
9.5
9.0
8.5
8.0
7.5
7.0
6.5
6.0
5.5
5.0
4.5
4.0
3.5
3.0
2.5
2.0
1.5
1.0
0.5
f1 (ppm)